Identification of novel virus from vervet monkey in Zambia and analysis of its viral assembly

（ザンビアのバーベットモンキーからの新規ウイルスの同定と粒子形成機構の解析）

Hiroki Yamaguchi

Division of Molecular Pathobiology,

Research Center for Zoonosis Control,

Hokkaido University

Contents

List of abbreviations

a.a.	Amino acids
AelPyV1	African elephant polyomavirus 1
AGM	African green monkey
AGMPyV	African green monkey polyomavirus
AIDS	Acquired immune deficiency syndrome
BatPyV	Bat polyomavirus
BFDPyV	Budgerigar fledgling disease polyomavirus
BKV	BK polyomavirus
BLAST	Basic local alignment search tool
BoPyV	Bovine polyomavirus
bp	Base pair
BSA	Bovine serum albumin
C-terminal	Carboxyl-terminal
CaPyV	Canary polyomavirus
cDNA	complementary deoxyribonucleic acid
ChPyV	Chimpanzee polyomavirus
CrPyV	Crow polyomavirus
CslPyV	California sea lion polyomavirus
Δ	Deletion mutant
DAPI	4′,6-diamidino-2-phenylindole
DDBJ	DNA Data Bank of Japan
DNA	Deoxyribonucleic acid
dpt	Days post transfection

DPyV1	Dolphin polyomavirus 1
E. coli	*Escherichia coli*
EDTA	Ethylenediaminetetracetic acid
EMBL	European Molecular Biology Laboratory
EqPyV	Equine polyomavirus
FBS	Fetal bovine serum
FiPyV	Finch polyomavirus
GggPyV	Gorilla gorilla gorilla polyomavirus
GHPyV	Goose hemorrhagic polyomavirus
H&E	Hematoxylin and eosin
HaPyV	Hamster polyomavirus
HEK	Human embryonic kidney
HRP	Horseradish peroxidase
HPyV	Human polyomavirus
IARC	International Agency for Research on Cancer
JCV	JC polyomavirus
KIV	KI polyomavirus
MasPyV	Mastomys polyomavirus
MCC	Merkel cell carcinoma
MCPyV	Merkel cell polyomavirus
MEGA 5 Beta	Molecular evolutionary genetics analysis version 5 beta
MPtV	Murine pneumotropic virus
mRNAs	messenger ribonucleic acids
MuPyV	Murine polyomavirus
MWPyV	MW polyomavirus

MXPyV	MX polyomavirus
MyoPyV	Myotis polyomavirus
N-terminal	Amino-terminal
NHPs	Nonhuman primates
OraPyV	Orangutan polyomavirus
ORF	Open reading frame
PBS	Phosphate buffered saline
PCR	Polymerase chain reaction
PML	Progressive multifocal leukoencephalopathy
PrufPyV	Piliocolobus rufomitratus polyomavirus
PtvPyV	Pan troglodytes verus polyomavirus
PyVs	Polyomaviruses
RNA	Ribonucleic acid
RT	Reverse transcription
RT-PCR	Reverse transcriptase-polymerase chain reaction
SA12	Simian agent 12
SDS	Sodium dodecyl sulfate
SDS-PAGE	Sodium dodecyl sulfate-polyacrylamide gel electrophoresis
SquiPyV	Squirrel monkey polyomavirus
STLPyV	STL polyomavirus
SV40	Simian virus 40
tAg	small T antigen
TAg	Large T antigen
TBST	Tris-buffered saline containing 0.05% Tween 20
TEM	Transmission electron microscopy

TSV	Trichodysplasia spinulosa-associated polyomavirus
VLPs	Virus-like particles
VMKs	Vervet monkey kidneys
VmPyV	Vervet monkey polyomavirus
VMs	Vervet monkeys
VMSs	Vervet monkey spleens
WT	Wild-type
WUV	WU polyomavirus
YBKs	Yellow baboon kidneys
YbPyV	Yellow baboon polyomavirus
YBs	Yellow baboons
YBSs	Yellow baboon spleens
ZAWA	Zambia Wildlife Authority

General Introduction

Polyomaviruses (PyVs), members of the family *Polyomaviridae*, are nonenveloped viruses carrying a circular double-stranded deoxyribonucleic acid (DNA) genome that is approximately 5,000 base pairs (bp) in size. PyV genomes consist of three functional regions: an early coding region, a late coding region, and a transcriptional control region. The early coding region encodes the regulatory proteins, including small t antigen (tAg) and large T antigen (TAg), which are necessary for viral genome replication and viral gene transcription, also known as tumour antigens. The late coding region mainly encodes the structural proteins, such as VP1, VP2, and VP3. The transcriptional control region contains replication origin and promoter and enhancer sequences, and regulates the replication of the viral genome and bidirectional viral transcription for both early and late genes (Imperiale & Major, 2007).

Murine PyV (MuPyV) was the first PyV discovered in 1953 while studying leukemia in mice (Ramqvist & Dalianis, 2009). The next member of the family to be isolated was simian virus 40 (SV40). SV40 was identified as a contaminant in monkey kidney cultures used to prepare the first poliovirus vaccine. This vaccine led to the exposure of an estimated 100 million people to SV40 (Klein *et al.*, 2002).

For human PyVs, BK PyV (BKV) was the first PyV isolated from the urine sample of a renal transplant patient, and JC PyV (JCV) was isolated from the brain tissue of a patient with progressive multifocal leukoencephalopathy (PML) (Imperiale & Major, 2007). Up to date, twelve human PyVs have been reported (Korup *et al.*, 2013).

Seroepidemiological studies were performed to confirm the presence of PyVs in the human population using virus-like particles (VLPs), prepared from recombinant VP1 (Kean *et al.*, 2009; Sroller *et al.*, 2013). This study showed that around 80% of

adults in the United States and Europe tested positive for BKV and JCV. It means that these PyVs are very common in the global population. Seroprevalence data suggested that these PyVs infection occurred during early childhood and that PyVs were ubiquitous among adults. These data also suggest that PyVs have coevolved with humans (Krumbholz *et al.*, 2009).

Although the infection of PyVs frequently occurs early in childhood among individuals living together, the distribution and transmission routes of PyVs remain unclear. There are some reports that PyVs DNA was detected in urban sewage systems (Sroller *et al.*, 2013). Thus, it may also be spread by fecal–oral route of transmission or a respiratory route (Bofill-Mas *et al.*, 2010). In fact, BKV DNA is found infrequently in the urine of healthy adults. Meanwhile, JCV viruria occurs universally, increasing with age, with adult prevalence rates often between 20% and 60% (Knowles, 2006).

Some of human PyVs cause subclinical infections with lifelong persistence in their natural nonimmunocompromised hosts. In particular in host immunity-compromised acquired immune deficiency syndrome (AIDS) patients and organ transplant recipients, the viruses can be reactivated and cause diseases such as nephropathy and cystitis, and PML (Jiang *et al.*, 2009). Moreover, JCV and BKV are classified as Group 2B (possibly carcinogenic to humans) by the International agency for research on cancer (IARC) (http://monographs.iarc.fr/ENG/Classification/).

Because diagnostic tools to detect viral genomes have been improved, many novel PyVs have been reported recently. Among the detected PyVs, some has pathogenicity to humans or nonhumans, such as birds and mammals except for humans. It is controversial as to whether PyVs can be transmitted from nonhumans to humans, or humans to nonhumans, and thereafter cause diseases. To examine potential threats of the zoonotic transfer of PyVs between humans and nonhumans, the surveillance of

PyVs in wildlife is important. In the current study, I examined PyVs in nonhuman primates (NHPs) in collaboration with the University of Zambia under permission from the Zambia Wildlife Authority (ZAWA).

In chapter 1, I examined the presence of PyVs in NHPs in Zambia and identified five full-length PyV genomes, one of which was found to be a novel PyV.

In chapter 2, I focused on characterization of a novel PyV. To test whether the novel PyV genome could produce viral proteins in cultured cells, the whole circular genome was transfected into mammalian cells. Furthermore, I generated VLPs to examine the role of the novel PyV VP1 in virion formation.

In this thesis, I investigated PyVs from NHPs in Zambia. This study provides information about the PyV prevalence in NHPs in Zambia and function of the carboxyl (C)-terminal region of a novel PyV VP1 in virion formation.

Chapter 1

Surveillance of polyomaviruses from nonhuman primates in Zambia

Introduction

PyVs carry a circular double-stranded DNA genome of approximately 5,000 bp and consisting of an early and a late coding region. Viral transcription is bidirectional from the origin of replication, which lies within the noncoding, regulatory region. The early coding region encodes tAg and TAg, whereas the late coding region encodes VP1, VP2, and VP3. Some PyVs also carry an agnoprotein gene upstream of the VP2 gene, which is thought to be associated with capsid assembly and enhancing viral release as a viroporin (Suzuki *et al.*, 2013; Suzuki *et al.*, 2010; Suzuki *et al.*, 2012); however, the function of agnoprotein is still unclear. In contrast, avian PyVs carry a VP4 gene, rather than the agnoprotein gene (Johne & Müller, 2007). VP4 interacts with the C-terminus of VP1 and may be incorporated into viral capsids (Shen *et al.*, 2011).

PyVs infect a broad range of birds and mammals, including humans. The advent of advanced molecular biology techniques including polymerase chain reaction (PCR), rolling circle amplification, and deep DNA sequencing led to the identification of many PyVs, including human and nonhuman PyVs. Twelve human PyVs have been identified to date: BKV, JCV, KI PyV [KIV; (Allander *et al.*, 2007)], WU PyV [WUV; (Gaynor *et al.*, 2007)], Merkel cell PyV [MCPyV; (Feng *et al.*, 2008)], human PyV 6 (HPyV6) and HPyV7 (Schowalter *et al.*, 2010), trichodysplasia spinulosa-associated PyV [TSV; (van der Meijden *et al.*, 2010)], HPyV9 (Scuda *et al.*, 2011), MW PyV (MWPyV)/HPyV10/MX PyV (MXPyV) (Buck *et al.*, 2012; Siebrasse *et al.*, 2012; Yu

et al., 2012), STL PyV [STLPyV; (Lim *et al.*, 2013)], and HPyV12 (Korup *et al.*, 2013). MWPyV, HPyV10, and MXPyV are probably different variants of a single species (Yu *et al.*, 2012). Not all of these human PyVs have been definitely linked to disease; however, some of these PyVs cause subclinical infections with life-long persistence in immunocompromised hosts. In particular in host immunity-compromised AIDS patients and organ transplant recipients, the viruses can reactivate and cause diseases (Jiang *et al.*, 2009). BKV causes nephropathy and cystitis, JCV causes PML, MCPyV was found to be specifically linked to Merkel cell carcinoma (MCC), a rare but aggressive form of skin cancer of neuroendocrine origin, and TSV was found in a patient with trichodysplasia spinulosa (Jiang *et al.*, 2009). Moreover, MCPyV was classified as "probably carcinogenic to humans" (Group 2A), and JCV and BKV were classified as "possibly carcinogenic to humans" (Group 2B) by IARC (http://monographs.iarc.fr/ENG/Classification/).

Nonhuman PyVs were identified from many species, such as bats, birds, elephants, horses, marine mammals, rodents, ruminants, and NHPs. The NHP PyVs simian agent 12 (SA12) and B-lymphotropic PyV were identified from the kidney cells of a vervet monkey (VM) and a lymphoblast cell line of an african green monkey (AGM), respectively (Cantalupo *et al.*, 2005; Pawlita *et al.*, 1985). Although SA12 was identified from an uninoculated vervet monkey kidney (VMK) culture, neutralizing antibodies to SA12 were more detectable in baboons (101/151; 67%) than in VMs (12/49; 24%) (Braun *et al.*, 1980). For this reason, the natural host of SA12 is thought to be baboons (Cantalupo *et al.*, 2005). SV40 was identified as a contaminant in monkey kidney cultures used to prepare the first poliovirus vaccine from the mid-1950s to 1963 (Klein *et al.*, 2002). On the basis of transformation activity of SV40 in human cells (Pipas, 2009), it has been suggested that SV40 infection occurring through the use of

contaminated vaccines may be a cause of some tumors in humans (Klein *et al.*, 2002). Indeed, SV40 DNA has been reported in a variety of human tumors, such as ependymomas, osteosarcomas, and mesotheliomas; however, the relationship between SV40 and these human tumors is still controversial (Bergsagel *et al.*, 1992; Lednicky *et al.*, 1995).

Some of the nonhuman PyVs related to diseases, especially birds PyVs are causative agents of acute diseases (i.e. hemorrhagic nephritis and hepatitis) with high mortality rates (Johne & Müller, 2007). It is controversial as to whether PyVs can be transmitted from NHPs to humans and thereafter cause disease. To examine potential threats of the zoonotic transfer of PyVs between humans and nonhumans, to avoid further risk of infection with unidentified PyVs, and to investigate their involvements in disease, the surveillance of PyVs in wildlife is important. In chapter 1, I examined the presence of PyVs in NHPs in Zambia using a nested broad-spectrum PCR-based assay targeting to VP1 region.

Materials and Methods

Sample collection and DNA extraction

Spleens and kidneys (n = 100 each) were collected from 50 yellow baboons (YBs; *Papio cynocephalus*) and 50 VMs (*Chlorocebus pygerythrus*) in the Mfuwe area (13°14′42.00″ S, 31°38′54.07″ E) in Zambia in 2009. DNA was extracted from these organs by using the QIAamp DNA Mini Kit (Qiagen, Valencia, CA) according to the manufacturer's instructions. Mitochondrial cytochrome *b* gene was sequenced for species identification using a forward primer (5′-GATACGAAAAACCATCGCTGT-3′) and a reverse primer (5′-GCTCCATTTCTGGTTTACAAG-3′) for YBs, and a forward primer (5′-TGATATGAAAAACCACCGTTGT-3′) and a reverse primer (5′-GCTTTCTTTCTGAGTTGTCCTAGG-3′) for VMs (Sasaki *et al.*, 2013). This study was authorized by ZAWA.

Detection of PyV genomes

To determine the presence of PyVs in extracted DNA samples, a nested broad-spectrum PCR method was performed to amplify PyV VP1 by using degenerate primers (Johne *et al.*, 2005; Orba *et al.*, 2011). A nested PCR was performed using 100 ng of extracted DNA and the High Fidelity PCR Master (Roche Diagnostics, Indianapolis, IN) in 20 μL of reaction mixtures. The first round of PCR amplification was as follows: 2 min of denaturation at 95°C, followed by 45 cycles of 94°C for 30 sec, 46°C for 1 min, and 72°C for 1 min, and a final extension step at 72°C for 5 min. For the second amplification reaction, 0.5 μL of the first PCR product was used as the template, and the same cycling protocol was used, except that the annealing step was

carried out at 56°C.

Sequence and phylogenetic analyses

PCR products resolved and visualized on ethidium bromide-stained 1.5% agarose gel electrophoresis were purified, subcloned into the pCR4-TOPO vector (Invitrogen, Carlsbad, CA), and then sequenced using the BigDye Terminator v3.0 Cycle Sequencing on the ABI PRISM 3130 Genetic Analyzer (Applied Biosystems, Foster City, CA). After sequencing, a similarity search was performed with a basic local alignment search tool (BLAST). The whole PyV genomes were obtained by inverse PCR using the PrimeSTAR GXL DNA Polymerase (Takara, Otsu, Japan) and primers facing outwards from the initial PCR VP1 gene products. Inverse PCR cycling protocol comprised 2 min of denaturation at 94°C: followed by 40 cycles of 98°C for 10 sec, 60°C for 15 sec, and 68°C for 5 min, and a final extension step at 68°C for 5 min. Each whole PyV genome was then subcloned into the pCR4-TOPO vector and sequenced.

Amino acid sequences of the following reference viral genomes were obtained from the GenBank: African elephant PyV 1 (AelPyV1), AGM PyV (AGMPyV), Bat PyV [BatPyV2a (AT7), BatPyV2b (R26F6), BatPyV2c (A504), BatPyV3a (A1055), BatPyV3a (B0454), BatPyV3b (B1130), BatPyV4a (R104), BatPyV4b (C1109)], BKV, Bovine PyV (BoPyV), Budgerigar fledgling disease PyV (BFDPyV), California sea lion PyV (CslPyV), Canary PyV (CaPyV), Chimpanzee PyV (ChPyV-Az, ChPyV-Bob, ChPyV-Ta), Crow PyV (CrPyV), Dolphin PyV 1 (DPyV1), Equine PyV (EqPyV), Finch PyV (FiPyV), Goose hemorrhagic PyV (GHPyV), Gorilla gorilla gorilla PyV (GggPyV), Hamster PyV (HaPyV), HPyV6, HPyV7, HPyV9, HPyV10, HPyV12, JCV, KIV, Mastomys PyV (MasPyV), MCPyV, Murine pneumotropic virus (MPtV),

MuPyV, Myotis PyV (MyoPyV), MWPyV, Orangutan PyV (OraPyV-Bor, OraPyV-Sum), Pan troglodytes verus PyV [PtvPyV1a (6444), PtvPyV1b (6520), PtvPyV2a (6512), PtvPyV2c (5924), PtvPyV2c (5927), PtvPyV2c (6413)], Piliocolobus rufomitratus PyV 1 (PrufPyV1), SA12, STLPyV, SV40, Squirrel monkey PyV (SquiPyV), TSV, and WUV (abbreviations and GenBank accession numbers can be found in Table 1). Multiple sequence alignments of the predicted tAg, TAg, VP1, and VP2 open reading frames (ORFs) were carried out using the Molecular evolutionary genetics analysis version 5 beta (MEGA 5 Beta) (Tamura *et al.*, 2011). The phylogenetic analysis was performed by using the neighbour-joining method with 1,000 bootstrap replicates (Felsenstein, 1985; Saitou & Nei, 1987). Phylogenetic trees were also generated using the MEGA 5 Beta (Tamura *et al.*, 2011).

Histological examination

The harvested tissues: brain, kidney, liver, lung, and spleen were fixed in 10% phosphate-buffered formalin (pH 7.2) and embedded in paraffin. Histological sections with a thickness of 3 μm were prepared from paraffin-embedded tissues and stained using Carrazzi's hematoxylin and eosin (H&E) (Kobayashi *et al.*, 2012).

Accession numbers

The GenBank/EMBL/DDBJ accession numbers for the complete nucleotide sequences of the PyVs determined in this study are AB767294, AB767295, and AB767297–AB767299 (Yamaguchi *et al.*, 2013).

Table 1. Abbreviations and accession numbers of protein sequences of referenced PyVs.

Polyomaviruses (PyVs)	Abbreviations	tAg	TAg	VP1	VP2
African elephant PyV 1	AelPyV1	AGV77096	AGV77095	AGV77094	AGV77092
African green monkey PyV	AGMPyV	NP_848009	NP_848008	NP_848007	NP_848005
Bat PyV 2a (AT7)	BatPyV2a (AT7)	AFP94208	AFP94207	AFP94206	AFP94205
Bat PyV 2b (R266)	BatPyV2b (R266)	AFP94204	AFP94203	AFP94202	AFP94201
Bat PyV 2c (A504)	BatPyV2c (A504)	AFP94200	AFP94199	AFP94198	AFP94197
Bat PyV 3a (A1055)	BatPyV3a (A1055)	AFP94183	AFP94182	AFP94181	AFP94180
Bat PyV 3a (B0454)	BatPyV3a (B0454)	AFP94192	AFP94191	AFP94190	AFP94189
Bat PyV 3b (B1130)	BatPyV3b (B1130)	AFP94212	AFP94211	AFP94210	AFP94209
Bat PyV 4a (R104)	BatPyV4a (R104)	AFP94188	AFP94187	AFP94186	AFP94185
Bat PyV 4b (C1109)	BatPyV4b (C1109)	AFP94196	AFP94195	AFP94194	AFP94193
BK PyV	BKV	CAA24301	CAA24300	CAA24299	CAA24297
Bovine PyV	BoPyV	NP_040789	NP_040788	NP_040787	NP_040785
Budgerigar fledgling disease PyV	BFDPyV	ADC34629	ADC34628	ADC34627	ADC34625
California sea lion PyV	CslPyV	ADC34412	ADC34413	ADC34409	ADC34410
Canary PyV	CaPyV	ADM88651	ADM88652	ADM88650	ADM88648
Chimpanzee PyV (Azzie)	ChPyV-Az	CBX23451	CBX23452	CBX23450	CBX23448
Chimpanzee PyV (Bob)	ChPyV-Bob	CBX23440	CBX23439	CBX23438	CBX23436
Chimpanzee PyV (Tanu)	ChPyV-Ta	CBX23446	CBX23445	CBX23444	CBX23442
Crow PyV	CrPyV	ABB04267	ABB04268	ABB04276	ABB04274
Dolphin PyV 1	DPyV1	AGR44743	AGR44742	AGR44739	AGR44740
Equine PyV	EqPyV	YP_006383693	YP_006383692	YP_006383691	YP_006383689
Finch PyV	FiPyV	ABB04273	ABB04274	ABB04271	ABB04270
Goose hemorrhagic PyV	GHPyV	NP_849171	NP_849170	NP_849169	NP_849167
Gorilla gorilla gorilla PyV	GggPyV	ADQ54206	ADQ54205	ADQ54207	ADQ54208
Hamster PyV	HaPyV	AAA67116	AAA67118	AAA67119	AAA67121
Human PyV 6	HPyV6	YP_003848920	YP_003848919	YP_003848918	YP_003848916
Human PyV 7	HPyV7	YP_003848925	YP_003848924	YP_003848923	YP_003848921
Human PyV 9	HPyV9	YP_004243707	YP_004243706	YP_004243705	YP_004243703
Human PyV 12	HPyV12	AGH58116	AGH58117	AGH58115	AGH58113
JC PyV	JCV	AAA82103	AAA82102	AAA82101	AAA82099

Table 1. Abbreviations and accession numbers of protein sequences of referenced PyVs (continued).

Polyomaviruses (PyVs)	Abbreviations	tAg	TAg	VP1	VP2
KI PyV	KIV	ABN09920	ABN09921	ABN09917	ABN09918
Mastomys PyV	MasPyV	BAJ53088	BAJ53087	BAJ53086	BAJ53084
Merkel cell PyV	MCPyV	YP_001651047	ACI25294	YP_001651048	YP_001651049
Murine pneumotropic virus	MPtV	ABM67406	ABM67405	ABM67407	ABM67408
Murine PyV	MuPyV	AAA46874	AAA46872	AAA46875	AAA46877
MW PyV	MWPyV	AFN02457	AFN02458	AFN02454	AFN02455
Myotis PyV	MyoPyV	YP_002261490	YP_002261489	YP_002261488	YP_002261486
Orangutan PyV (Borneo)	OraPyV-Bor	CAX87752	CAX87750	CAX87748	CAX87744
Orangutan PyV (Sumatra)	OraPyV-Sum	CAX87761	CAX87759	CAX87757	CAX87754
Pan troglodytes verus PyV 1a (6444)	PtvPyV1a (6444)	ADQ54179	ADQ54175	ADQ54176	ADQ54177
Pan troglodytes verus PyV 1b (6520)	PtvPyV1b (6520)	ADQ54181	ADQ54180	ADQ54182	ADQ54183
Pan troglodytes verus PyV 2a (6512)	PtvPyV2a (6512)	ADQ54186	ADQ54185	ADQ54187	ADQ54188
Pan troglodytes verus PyV 2c (5924)	PtvPyV2c (5924)	ADQ54191	ADQ54190	ADQ54192	ADQ54193
Pan troglodytes verus PyV 2c (5927)	PtvPyV2c (5927)	ADQ54196	ADQ54195	ADQ54197	ADQ54198
Pan troglodytes verus PyV 2c (6413)	PtvPyV2c (6413)	ADQ54201	ADQ54200	ADQ54202	ADQ54203
Piliocolobus rufomitratus PyV 1	PrufPyV1	AFU25599	AFU25598	AFU25596	AFU25597
Simian agent 12	SA12	AAV75980	AAV75979	AAV75982	AAV75983
Simian virus 40	SV40	AAB59925	AAB59924	AAB59923	AAB59921
Squirrel monkey PyV	SquPyiV	YP_001531350	YP_001531349	YP_001531348	YP_001531346
STL PyV	STLPyV	AGC03172	AGC03170	AGC03169	AGC03167
Trichodysplasia spinulosa-associated PyV	TSV	YP_003800008	YP_003800007	YP_003800006	YP_003800004
Vervet monkey PyV 1	VmPyV1	BAM71870	BAM71869	BAM71868	BAM71866
Vervet monkey PyV 2	VmPyV2	BAM71876	BAM71875	BAM71874	BAM71872
Vervet monkey PyV 3	VmPyV3	BAM71865	BAM71864	BAM71863	BAM71861
WU PyV	WUV	ABQ09293	ABQ09292	ABQ09289	ABQ09290
Yellow baboon PyV 1	YbPyV1	BAM71848	BAM71847	BAM71846	BAM71844
Yellow baboon PyV 2	YbPyV2	BAM71854	BAM71853	BAM71852	BAM71850

Results

Detection of PyVs in spleens and kidneys from YBs and VMs

Under the permission from ZAWA, members of our laboratory collected spleens and kidneys (n = 100 each) from 50 YBs (*Papio cynocephalus*) and 50 VMs (*Chlorocebus pygerythrus*) in the Mfuwe area in Zambia in 2009. In total, 200 DNA samples were extracted and screened for the presence of PyV sequences by using a nested broad-spectrum PCR method with degenerate primers targeting the PyV VP1 region. The PCR results showed the presence of positive bands approximately 250 bp in seven out of 200 DNA samples (3.5%), including two from yellow baboon spleens (YBSs), one from yellow baboon kidneys (YBKs), three from vervet monkey spleens (VMSs), and one from VMKs (Table 2).

The PCR products were subsequently sequenced and analyzed by a BLAST search. The BLAST search demonstrated that six DNA sequences were approximately 90% homologous at the nucleotide level with the VP1 region of either AGMPyV or SA12, whereas one sample (VMS96) showed only 74% nucleotide homology with the VP1 region of ChPyV (Deuzing *et al.*, 2010) (Table 2). Among 50 YBs and 50 VMs, one YB and one VM contained PyV genomes in both the spleen and kidney (Table 2).

Whole viral genome analysis

Next, I identified whole viral genomes of these seven detected PyV fragments by an inverse PCR method using primers designed on the basis of the PCR-amplified VP1 nucleotide sequences described above. The whole PyV genome sequences were then determined, whose sizes are approximately 5,000 bp (Table 2). I found YBS94 and YBK94 to have an identical sequence of 5,181 bp (Yellow baboon polyomavirus 2;

Table 2. Profile of PyV genomes identified from the spleens and kidneys of YBs and VMs in Zambia.

No.	Abbreviations	Species	Organs	Closely related viruses and similarities (%) at the nucleotide level with the VP1		Full length of genomes (bp)	Accession numbers
YBS20	YbPyV1	Yellow baboon (*Papio cynocephalus*)	Spleen	AGMPyV	87%	5,064	AB767294
YBS94	YbPyV2	Yellow baboon (*Papio cynocephalus*)	Spleen	SA12	94%	5,181	AB767295
YBK94			Kidney				
VMS96	VmPyV1	Vervet monkey (*Chlorocebus pygerythrus*)	Spleen	ChPyV	74%	5,157	AB767298
VMK96	VmPyV2		Kidney	SA12	88%	5,167	AB767299
VMS95	VmPyV3	Vervet monkey (*Chlorocebus pygerythrus*)	Spleen	AGMPyV	94%	5,055	AB767297
VMS97		Vervet monkey (*Chlorocebus pygerythrus*)					

YbPyV2). Also, VMS95 and VMS97 have an identical sequence of 5,055 bp (Vervet monkey polyomavirus 3; VmPyV3). All these viral genomes have a typical set of PyV ORFs for the early (tAg and TAg) and late (VP1 and VP2/3) proteins, and those obtained from YbPyV2 and VMK96 (VmPyV2) carry the genes encoding for agnoprotein, whereas the other three (YbPyV1, VmPyV1, and VmPyV3) do not.

I also confirmed the whole PyV genome sequences using a different method. I designed individual primer sets facing outwards in the VP2/3 region from the obtained sequences against a different region from the initial VP1 gene product, and tried to detect PyV genomes from the DNA samples isolated from tissues by using an inverse PCR method. I detected the PyV genome from each sample, and purified it from agarose gel and then directly sequenced the full genome. The complete nucleotide sequences of the PyVs have been deposited in the GenBank database under the following accession numbers: for YBS20 (YbPyV1), AB767294; for YbPyV2, AB767295; for VMS96 (VmPyV1), AB767298; for VmPyV2, AB767299; and for VmPyV3, AB767297.

Phylogenetic analysis of 5 identified viral genomes

Phylogenetic trees of the PyV proteins (tAg, TAg, VP1, and VP2) that were constructed by the neighbour-joining method suggest that all the analyzed early (tAg and TAg) and late (VP1 and VP2) proteins of YbPyV2 and VmPyV3 are closely related to those of AGMPyV and HPyV9 (Fig. 1A-D). YbPyV2 and VmPyV2 were also found to be more closely related to SA12, BKV, JCV, and SV40 than to other known PyVs. Although VmPyV1 and VmPyV2 were identified from the same animal, viral proteins of VmPyV2 are closely related to those of SA12, whereas viral proteins of VmPyV1 are related to those of ChPyV and MCPyV. These results suggest that the

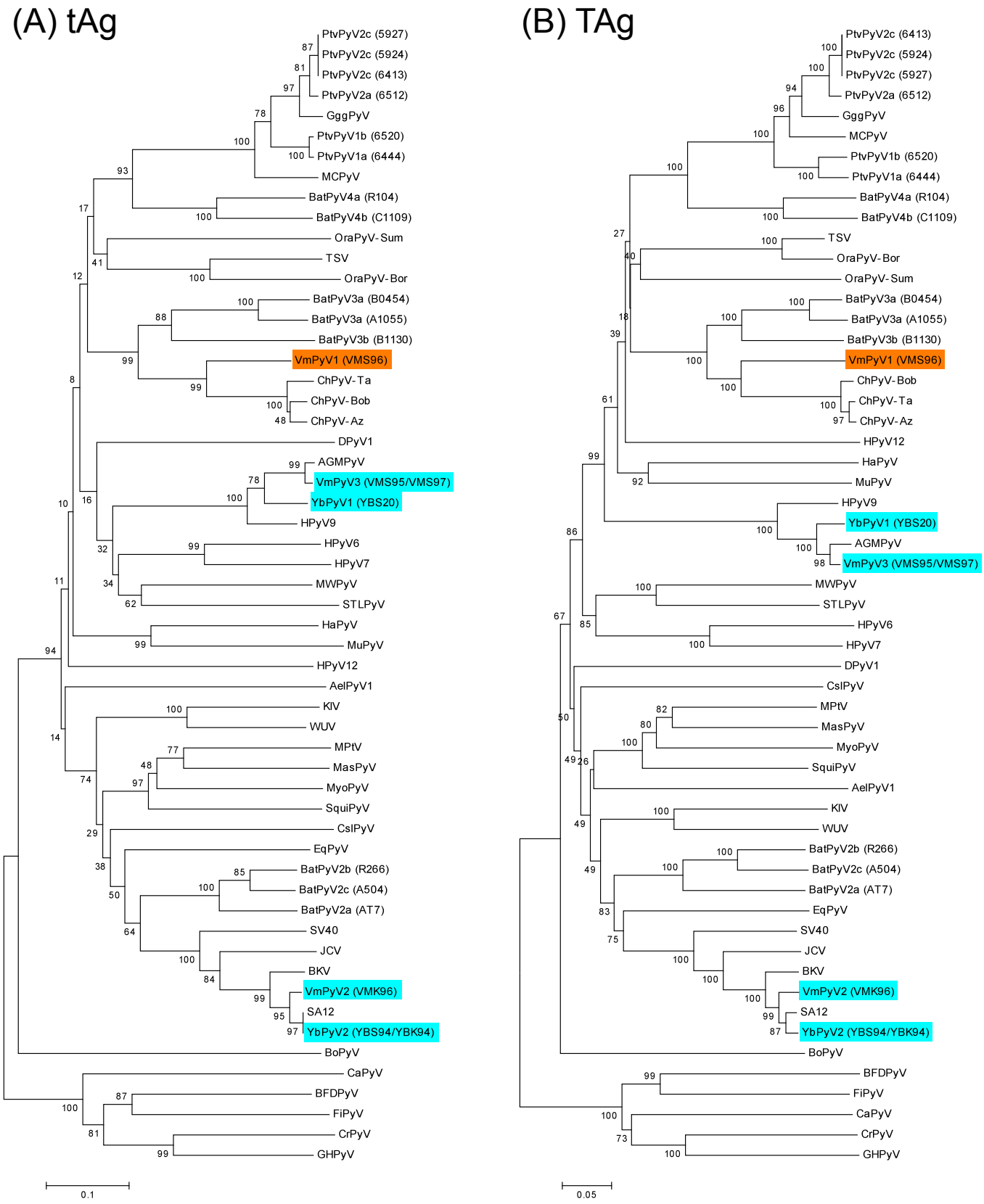
(A) tAg
PtvPyV2c (5927)
PtvPyV2c (5924)
PtvPyV2c (6413)
PtvPyV2a (6512)
GggPyV
PtvPyV1b (6520)
PtvPyV1a (6444)
MCPyV
BatPyV4a (R104)
BatPyV4b (C1109)
OraPyV-Sum
TSV
OraPyV-Bor
BatPyV3a (B0454)
BatPyV3a (A1055)
BatPyV3b (B1130)
VmPyV1 (VMS96)
ChPyV-Ta
ChPyV-Bob
ChPyV-Az
DPyV1
AGMPyV
VmPyV3 (VMS95/VMS97)
YbPyV1 (YBS20)
HPyV9
HPyV6
HPyV7
MWPyV
STLPyV
HaPyV
MuPyV
HPyV12
AelPyV1
KIV
WUV
MPtV
MasPyV
MyoPyV
SquiPyV
CslPyV
EqPyV
BatPyV2b (R266)
BatPyV2c (A504)
BatPyV2a (AT7)
SV40
JCV
BKV
VmPyV2 (VMK96)
SA12
YbPyV2 (YBS94/YBK94)
BoPyV
CaPyV
BFDPyV
FiPyV
CrPyV
GHPyV
0.1
(B) TAg
PtvPyV2c (6413)
PtvPyV2c (5924)
PtvPyV2c (5927)
PtvPyV2a (6512)
GggPyV
MCPyV
PtvPyV1b (6520)
PtvPyV1a (6444)
BatPyV4a (R104)
BatPyV4b (C1109)
TSV
OraPyV-Bor
OraPyV-Sum
BatPyV3a (B0454)
BatPyV3a (A1055)
BatPyV3b (B1130)
VmPyV1 (VMS96)
ChPyV-Bob
ChPyV-Ta
ChPyV-Az
HPyV12
HaPyV
MuPyV
HPyV9
YbPyV1 (YBS20)
AGMPyV
VmPyV3 (VMS95/VMS97)
MWPyV
STLPyV
HPyV6
HPyV7
DPyV1
CslPyV
MPtV
MasPyV
MyoPyV
SquiPyV
AelPyV1
KIV
WUV
BatPyV2b (R266)
BatPyV2c (A504)
BatPyV2a (AT7)
EqPyV
SV40
JCV
BKV
VmPyV2 (VMK96)
SA12
YbPyV2 (YBS94/YBK94)
BoPyV
BFDPyV
FiPyV
CaPyV
CrPyV
GHPyV
0.05

(C) VP1

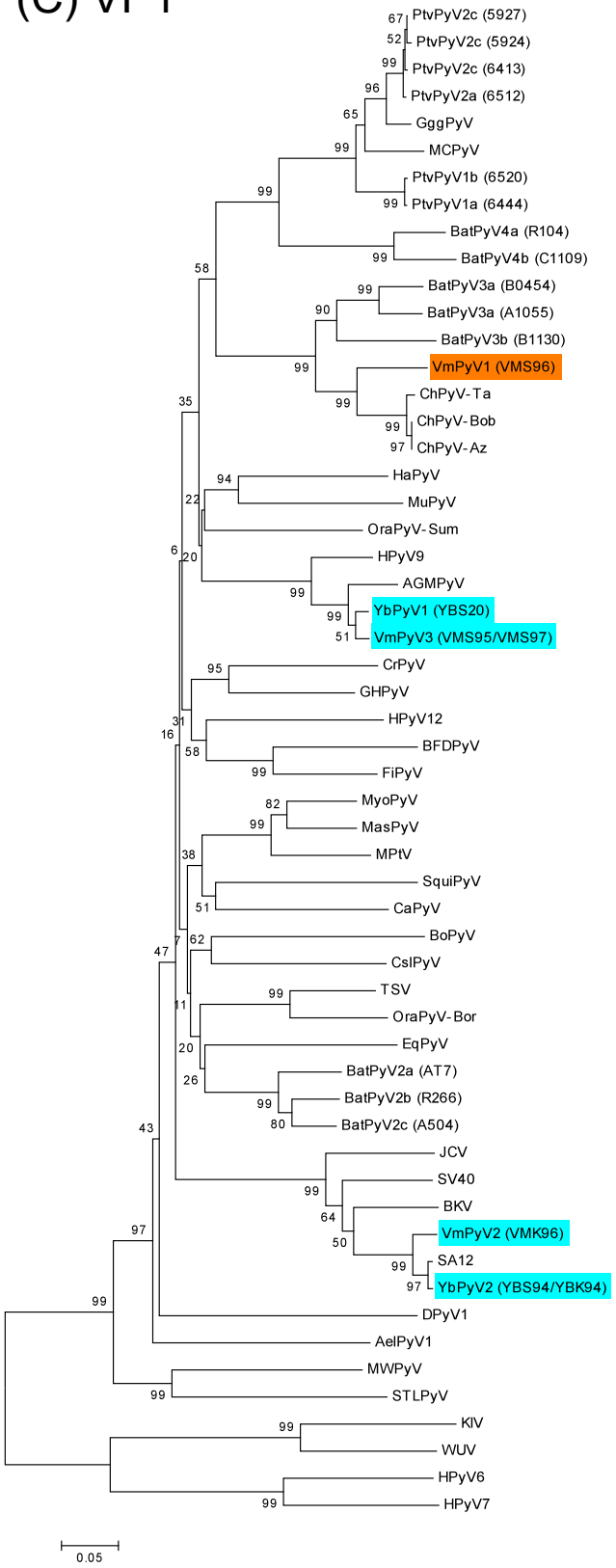
PtvPyV2c (5927)
PtvPyV2c (5924)
PtvPyV2c (6413)
PtvPyV2a (6512)
GggPyV
MCPyV
PtvPyV1b (6520)
PtvPyV1a (6444)
BatPyV4a (R104)
BatPyV4b (C1109)
BatPyV3a (B0454)
BatPyV3a (A1055)
BatPyV3b (B1130)
VmPyV1 (VMS96)
ChPyV-Ta
ChPyV-Bob
ChPyV-Az
HaPyV
MuPyV
OraPyV-Sum
HPyV9
AGMPyV
YbPyV1 (YBS20)
VmPyV3 (VMS95/VMS97)
CrPyV
GHPyV
HPyV12
BFDPyV
FiPyV
MyoPyV
MasPyV
MPtV
SquiPyV
CaPyV
BoPyV
CslPyV
TSV
OraPyV-Bor
EqPyV
BatPyV2a (AT7)
BatPyV2b (R266)
BatPyV2c (A504)
JCV
SV40
BKV
VmPyV2 (VMK96)
SA12
YbPyV2 (YBS94/YBK94)
DPyV1
AelPyV1
MWPyV
STLPyV
KIV
WUV
HPyV6
HPyV7
0.05

(D) VP2

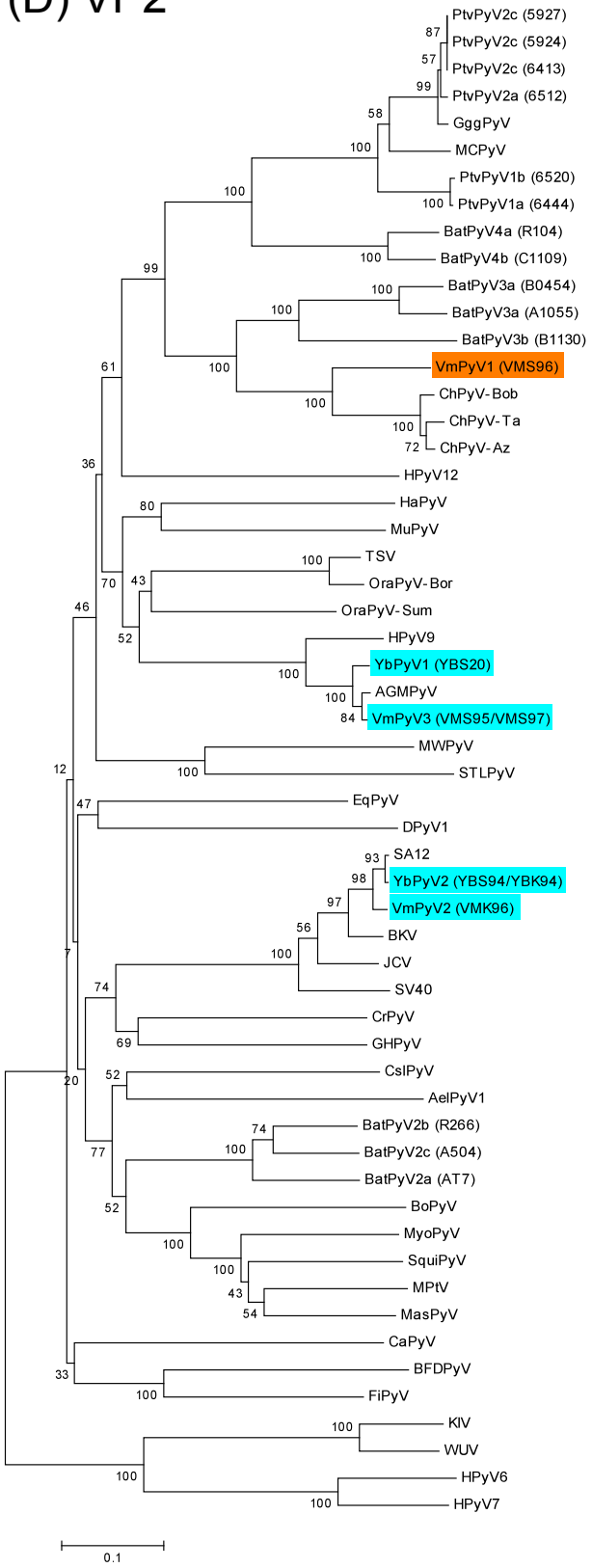
PtvPyV2c (5927)
PtvPyV2c (5924)
PtvPyV2c (6413)
PtvPyV2a (6512)
GggPyV
MCPyV
PtvPyV1b (6520)
PtvPyV1a (6444)
BatPyV4a (R104)
BatPyV4b (C1109)
BatPyV3a (B0454)
BatPyV3a (A1055)
BatPyV3b (B1130)
VmPyV1 (VMS96)
ChPyV-Bob
ChPyV-Ta
ChPyV-Az
HPyV12
HaPyV
MuPyV
TSV
OraPyV-Bor
OraPyV-Sum
HPyV9
YbPyV1 (YBS20)
AGMPyV
VmPyV3 (VMS95/VMS97)
MWPyV
STLPyV
EqPyV
DPyV1
SA12
YbPyV2 (YBS94/YBK94)
VmPyV2 (VMK96)
BKV
JCV
SV40
CrPyV
GHPyV
CslPyV
AelPyV1
BatPyV2b (R266)
BatPyV2c (A504)
BatPyV2a (AT7)
BoPyV
MyoPyV
SquiPyV
MPtV
MasPyV
CaPyV
BFDPyV
FiPyV
KIV
WUV
HPyV6
HPyV7
0.1

Figure 1. Phylogenetic analysis of PyV-encoded proteins. Phylogenetic trees were constructed using the (A) tAg, (B) TAg, (C) VP1, and (D) VP2 proteins. The PyVs identified in this thesis are highlighted by orange (VmPyV1) and aqua color (VmPyV2, VmPyV3, YbPyV1, and YbPyV2). The sequences of other reference PyVs were obtained from GenBank (abbreviations and accession numbers are indicated in Table 1). Phylogenetic analysis was performed by the neighbour-joining method with 1,000 bootstrap replicates, with percentages indicated on the nodes. Bars, amino acid residue replacements per site.

same VM was coinfected with different PyVs.

Interestingly, the VP1 region of the VmPyV1 genome shares low nucleotide homology (74%) with that of ChPyV (Table 2). I found that not only VP1 but also other proteins of VmPyV1 shared low nucleotide homology with other PyVs such as SV40, MCPyV, and ChPyV. According to the low homology between VmPyV1 and other three PyVs (Table 3), VmPyV1 seems to be a novel virus. The VmPyV1 genome consists of typical PyV ORFs (tAg, TAg, VP1, and VP2), but not agnoprotein (Fig. 2). The alignment results also suggest that VmPyV1, like ChPyV, encodes the VP1 with extra 150 amino acids (a.a.) in its C-terminal tail, in contrast to other known PyVs. In summary, I identified five PyV genomes among the 200 DNA samples tested, and one of them (VmPyV1) is a novel PyV.

PCR and histological examination of VM96 tissues

Although I attempted to examine the presence of PyV genomes in other tissues (liver and lung) from VM96 using the same method, as I used to detect PyV genomes in the kidney and spleen, I failed to detect any PCR positive signals. In addition, histological analysis of tissues (brain, kidney, liver, lung, and spleen) from VM96 revealed that no noteworthy pathological findings in these tissues (Fig. 3).

Table 3. Comparison of viral protein sequence similarities (%) between VmPyV1 and the PyVs (SV40, MCPyV, and ChPyV).

	Amino acid sequence similarity (%)		
	SV40	MCPyV	ChPyV
tAg	34	42	70
TAg	38	45	74
VP1	51	51	77
VP2	17	46	77

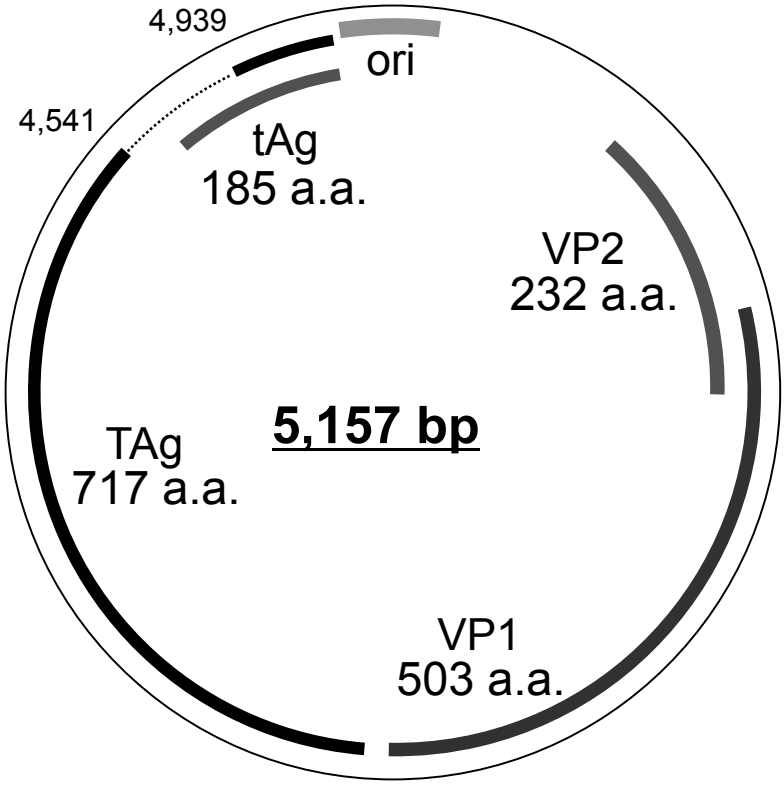

Figure 2. VmPyV1 genome organization. The whole VmPyV1 genome was 5,157 bp. The positions and number of amino acids for tAg, TAg, VP1, and VP2 are indicated. ori, Origin of replication. The dotted line indicates the predicted splicing site (nt 4,542–4,938).

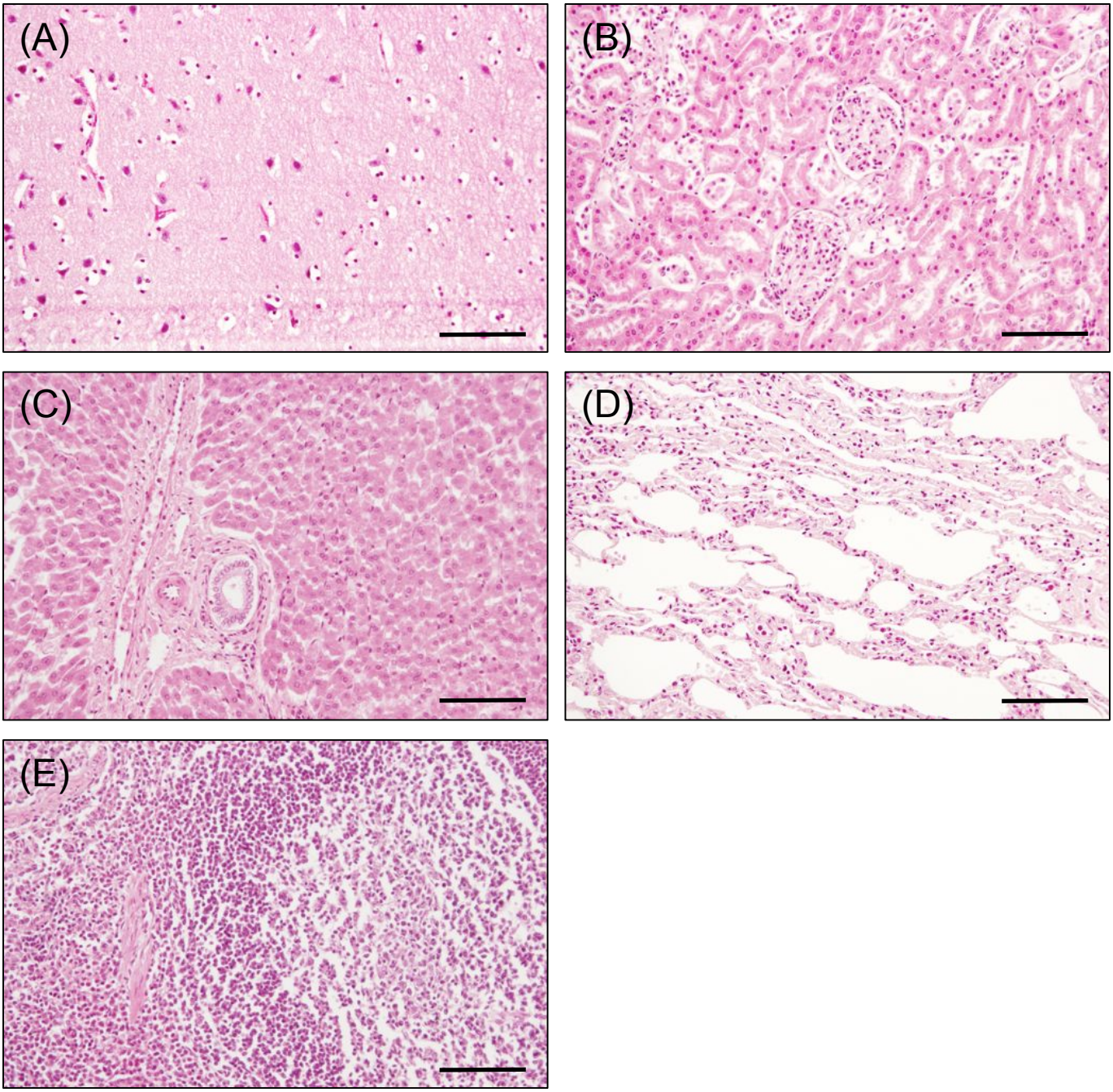

Figure 3. Histological analysis of the brain (A), kidney (B), liver (C), lung (D), and spleen (E) of VM96. Each section was stained with H&E. Bars, 100 μm.

Discussion

In chapter 1, five PyV genomes from wild YBs and VMs in Zambia were identified, four of which were shown to be closely related to AGMPyV and SA12, on the basis of the sequence and phylogenetic analyses of the full genomes and encoded proteins. These five PyVs were detected in spleens or kidneys of two YBs and three VMs, among 50 YBs and 50 VMs examined. In these four positive animals (YB20, YB94, VM95, and VM97), I also attempted to examine the presence of PyV genomes in other tissues, such as liver and lung; however, I did not obtain any positive findings.

On the basis of the phylogenetic analysis of viral proteins, VmPyV1 seems to be a novel PyV and is related to ChPyV and MCPyV. ChPyV has been identified in the faeces of chimpanzees (Deuzing *et al.*, 2010), whereas MCPyV has been identified from human MCC, which is a rare but aggressive type of skin cancer (Feng *et al.*, 2008). The genome structure of VmPyV1 comprises common ORF structures of PyVs, such as tAg, TAg, VP1, and VP2, but not agnoprotein (Fig. 2). Comparison with other PyVs also revealed that VmPyV1 encodes an unusually long VP1 of 503 a.a. Similarly, some PyVs possess longer VP1, such as PrufPyV1 [502 a.a.; (Scuda *et al.*, 2013)], ChPyV [497 a.a.; (Deuzing *et al.*, 2010)], CslPyV [495 a.a.; (Wellehan *et al.*, 2011)], BatPyV [472 a.a.; (Fagrouch *et al.*, 2012)], and MCPyV [423 a.a.; (Feng *et al.*, 2008)], whereas typical PyV VP1s have approximately 360 a.a. (SV40 VP1, 364 a.a., and JCV VP1, 354 a.a.). The alignment of VP1 from VmPyV1 and SV40, MCPyV, and ChPyV are shown in (Table 3). Interestingly, according to a previous report, in which ChPyV VP1 was expressed in yeast cells, the diameter of generated VLPs (approximately 45 nm) was the same as that of typical PyV particles, even though the ChPyV VP1 was 497 a.a. long. The results suggest that the number of amino acids is not related to the

diameter of virions (Zielonka *et al.*, 2011). However, the functions of this long C-terminal tail of VP1 are still unknown. Moreover, I performed PCR and histological analyses of tissues from VM96, and found that there were no positive signals in PCR analysis, and no histological findings.

In the past few years, a number of PyVs have been identified in animals, including humans (Anthony *et al.*, 2013; Korup *et al.*, 2013; Scuda *et al.*, 2013; Stevens *et al.*, 2013; Yamaguchi *et al.*, 2013). African great apes have also been shown to be infected with PyVs that are closely related to MCPyV (Leendertz *et al.*, 2011), which has provided evidence for the hypothesis that PyVs can be transmitted between humans and wild animals. In some parts of rural Africa, because humans and NHPs may live in close proximity, an accidental contact between people and these animals can occur (Hockings *et al.*, 2010). Therefore, concern must be raised regarding close contact between humans and NHPs to avoid infection of pathogens, including PyVs. The surveillance of wildlife needs to be continued to examine the transmission possibility of infectious agents.

In conclusion, I detected PyV genomes from NHPs in Zambia and also identified a novel PyV from VMS, which was designated as a vervet monkey polyomavirus 1, VmPyV1.

In chapter 2, I focused on further characterization of the VmPyV1.

Summary

To examine PyV infection in wildlife, I investigated the presence of PyVs in Zambia with permission from the Zambia Wildlife Authority. I analyzed 200 DNA samples from the spleens and kidneys (n = 100 each) of YBs and VMs (n = 50 each). I detected seven PyV genome fragments in 200 DNA samples using a nested broad-spectrum PCR method, and identified five full-length viral genomes using an inverse PCR method. Phylogenetic analysis of virally encoded proteins revealed that four PyVs were closely related to either AGMPyV or SA12. Only one virus detected from a VMS was found to be related, with relatively low nucleotide sequence identity (74%), to the ChPyV, which shares 48% nucleotide sequence identity with the human MCPyV identified from MCC. The obtained entire genome of this virus was 5,157 bp and had tAg and TAg, and VP1 and VP2 ORFs. This virus was tentatively named vervet monkey PyV 1 (VmPyV1) as a novel PyV. Comparison with other PyVs revealed that VmPyV1, like ChPyV, had a longer VP1 ORF. In conclusion, I detected PyV genomes from NHPs in Zambia and also identified a novel PyV from a VMS, which was designated as VmPyV1.

Chapter 2

Analysis of vervet monkey polyomavirus 1

Introduction

In the past few years, novel human and nonhuman PyVs have been identified (Anthony *et al.*, 2013; Korup *et al.*, 2013; Orba *et al.*, 2011; Scuda *et al.*, 2013; Stevens *et al.*, 2013). In chapter 1 of this thesis, I identified a novel PyV, vervet monkey PyV 1 (VmPyV1), in a VM by using a nested broad-spectrum PCR method (Yamaguchi *et al*., 2013). The obtained entire VmPyV1 genome is 5,157 bp in size and has tAg, TAg, VP1, and VP2 ORFs. VmPyV1 genome encodes the unique extended C-terminal VP1 of 503 a.a., whereas typical PyVs such as SV40 and JCV genomes encode VP1s with lengths of 364 and 354 a.a., respectively (Yamaguchi *et al.*, 2013). VP1s with the long C-terminal regions are also observed in some other PyVs such as PrufPyV1 [502 a.a.; (Scuda *et al.*, 2013)], ChPyV [497 a.a.; (Deuzing *et al.*, 2010)], CslPyV [495 a.a.; (Wellehan *et al.*, 2011)], BatPyV [472 a.a.; (Fagrouch *et al.*, 2012)], and MCPyV [423 a.a.; (Feng *et al.*, 2008)].

The virions of PyVs are nonenveloped and icosahedral with a diameter of approximately 45-50 nm and an outer surface consisting mainly of the capsid protein VP1. The PyV capsid is formed by 72 VP1 pentamers, each of them is arranged in a T = 7 icosahedral lattice (Liddington *et al.*, 1991). Other capsid proteins, VP2 and VP3, extend from the core into the axial cavity of the pentamers. Although it has been reported that the C-terminal tail of VP1 extends out of the pentamer and contacts the neighboring pentamers (Kawano *et al.*, 2006; Liddington *et al.*, 1991; Stehle *et al.*,

1996), the function of the long C-terminal region of VmPyV1 VP1 is still unclear.

It is known that recombinant PyV VP1s expressed in *Escherichia coli* (*E. coli*), yeast cells, insect cells, or mammalian cells are able to self-assemble into VLPs without viral genomic DNA and VP2/VP3 (Chang *et al.*, 1997; Chen *et al.*, 2001; Kobayashi *et al.*, 2013; Ou *et al.*, 1999; Tolstov *et al.*, 2009; Zielonka *et al.*, 2011).

In chapter 2, I focused on a novel PyV, VmPyV1. To test whether the VmPyV1 genome produce viral proteins in cultured cells, the whole circular genome was transfected into mammalian cells. Moreover, I generated VmPyV1 VLPs and examined their morphology by using electron microscopy to determine the role of C-terminal region of VmPyV1 VP1 in virion formation.

Materials and Methods

Cells

HEK293T, a human embryonic kidney 293 cell line expressing SV40 TAg, cells were maintained under the condition: atmosphere of 5% CO_2 at 37°C in Dulbecco's minimum essential medium, supplemented with 10% fetal bovine serum (FBS), 2 mM L-glutamine, penicillin (100 U/ml), and streptomycin (0.1 mg/ml). All experiments using HEK293T cells were carried out in collagen-coated dishes (Iwaki, Chiba, Japan).

Transfection of VmPyV1 genome

The full VmPyV1 genome was subcloned into the *KpnI* site of pUC19 vector (pUC19-VmPyV1) (Clontech, Mountain View, CA). The pUC19-VmPyV1 was digested with *KpnI* (Takara), and the VmPyV1 genome was extracted from an agarose gel and purified using the MonoFas Column (GL Science, Tokyo, Japan). Purified DNA was self-ligated in the presence of T4 DNA ligase at 16°C overnight (Takara). Subsequently, DNA (2 μg) purified by the phenol-chloroform-isoamyl alcohol extraction method was transfected into HEK293T cells with the FuGENE HD according to the manufacturer's instructions (Roche Diagnostics).

Reverse transcription-PCR (RT-PCR)

At 4 days post-transfection (dpt) with the VmPyV1 genome, cells were lysed in the Trizol Reagent (Invitrogen) for ribonucleic acid (RNA) isolation. Total RNA was then subjected to reverse transcription by using random primers and the SuperScript III Reverse Transcriptase (Invitrogen). To detect VmPyV1 complementary DNA (cDNA), PCR was performed using the Takara Ex Taq in 20 μL of reaction mixtures (Takara).

TAg cDNA was amplified using a forward primer (5′-TCCACCTGCATGGCTAACTTCTG-3′) and a reverse primer (5′-GGAGCGAGTACTGCAAAAAAGTGAG-3′). The PCR conditions were as follows: 2 min of denaturation at 94°C, followed by 25 cycles of 98°C for 10 sec, 65°C for 30 sec, and 72°C for 1 min, and a final extension step at 72°C for 5 min. Similarly, to detect the late cording region for VP1 cDNA, PCR was performed using a forward primer (5′-TTCCACATGTTTGCTGTTGGGG-3′) and reverse primer (5′-TTCATGTCAGGGTCAGCTGGC-3′). PCR products visualized on ethidium bromide-stained 2% agarose gel were purified and then directly sequenced.

Immunocytochemical and immunoblot analyses

At 4 dpt, cells were washed with phosphate buffered saline (PBS), fixed in 100% methanol for 5 min at −30°C, and then blocked with 1% bovine serum albumin (BSA) in PBS with 0.5% Triton X-100, followed by incubation with the polyclonal anti-SV40 VP1 antibody overnight at 4°C (Kasamatsu & Nehorayan, 1979). Cells were visualized with secondary antibodies (Alexa Fluor 488 Goat Anti-rabbit IgG; Invitrogen) and 4′,6-diamidino-2-phenylindole dihydrochloride (DAPI; Invitrogen) for 1 hr at room temperature. Fluorescent images were captured and analyzed using a microscope (IX70; Olympus, Tokyo, Japan), charge-coupled device camera (DP30BW; Olympus), and DP Controller software (Olympus).

For immunoblot analysis, cells were harvested in lysis buffer [10 mM Tris-HCl (pH 7.5), 5 mM ethylenediaminetetraacetic acid (EDTA), 150 mM NaCl, 10% glycerol, 1% Triton X-100, 1% deoxycholic acid, 0.1% sodium dodecyl sulfate (SDS), 50 mM NaF], supplemented with complete protease inhibitor cocktail (Roche Diagnostics). Cell lysates were centrifuged at 20,400 × *g* at 4°C for 15 min, and resulting

supernatants were subjected to sodium dodecyl sulfate-polyacrylamide gel electrophoresis (SDS-PAGE) and then immunoblotting with the anti-SV40 VP1 antibody overnight at 4°C. After washing the membrane with TBST (Tris-buffered saline containing 0.05% Tween 20), the membrane was incubated with horseradish peroxidase-conjugated (HRP) anti-rabbit IgG for 1 hr at room temperature (Biosource International, Camarillo, CA). The chemiluminescence signals were visualized using a VersaDoc 5000MP (Bio-Rad, Hercules, CA), and images were analyzed using Quantity One software (Bio-Rad).

Plasmids and transfection for VmPyV1 VLPs

For expression of VmPyV1 VP1, the full-length VmPyV1 VP1 gene was amplified from the VmPyV1 genomic DNA (GenBank accession number; AB767298) with *XhoI* and *NotI* restriction sites added to the 5' and 3' ends, respectively. The PCR product was cloned into the *XhoI*-*NotI* restriction sites of a pCMV-FLAG vector, so that a FLAG tag was added to the amino (N)-terminal of expressed VP1. The C-terminal deletion mutant (1-387 a.a. residues of VmPyV1 VP1) (Δ) with a stop codon (TAA) was also amplified and cloned into the vector. These plasmids were transfected into HEK293T cells individually using the Lipofectamine 2000 according to the manufacturer's instructions (Invitrogen).

Immunocytochemical and immunoblot analyses for VmPyV1 VLPs

HEK293T cells transfected with the plasmids were collected at 2 dpt. The cells were washed with PBS, fixed in 100% methanol for 5 min at −30°C and blocked with 1% BSA in PBS containing 0.5% Triton X-100, followed by incubation with an anti-SV40 VP1 antibody overnight at 4°C. The cells were visualized with secondary

antibodies (Alexa Fluor 488-conjugated Goat Anti-rabbit IgG; Invitrogen) and DAPI (Invitrogen) for 1 hr at room temperature. All the fluorescent images were captured and analyzed using a microscope, a charge-coupled device camera, and DP Controller software (all from Olympus).

For immunoblot analysis, the cells were harvested in lysis buffer (described above), supplemented with complete protease inhibitor cocktail (Roche Diagnostics). Cell lysates were centrifuged at 20,400 × *g* for 15 min at 4°C, and the resulting supernatants were subjected to SDS-PAGE and immunoblotting with the following primary antibodies for overnight at 4°C: an anti-SV40 VP1 antibody and an anti-actin antibody (MAB1501; Millipore, Bedford, MA). Actin was used as a loading control. After washing the membrane with TBST, the membrane was incubated with the following secondary antibodies for 1 hr at room temperature: HRP-conjugated anti-rabbit IgG and HRP-conjugated anti-mouse IgG (both from Biosource International). The immune complexes were detected with Immobilon Western HRP Substrate (Millipore). The chemiluminescence signals were visualized using a VersaDoc 5000MP (Bio-Rad), and images were analyzed using Quantity One software (Bio-Rad).

Electron microscopy

Ultra-thin-section electron microscopy was performed as described previously (Noda *et al.*, 2002). In brief, 2 dpt cells were fixed with 2.5% glutaraldehyde in 0.1 M cacodylate buffer (pH 7.3) for 20 min at 4°C. The cells were scraped from the dish and fixed with 2% osmium tetroxide in the same buffer for 1 hr at 4°C. Pellets were dehydrated with a series of ethanol gradients (50%, 70%, 90%, and 99.5%) followed by propylene oxide, embedded in Epon 812 Resin mixture (TAAB Laboratories Equipment, Berkshire, England), and polymerized for 3 days at 60°C. Thin-sections

(70 nm) were stained with uranyl acetate and lead citrate.

For negative staining, purified fractions fixed with 0.25% glutaraldehyde were adsorbed to collodion-carbon-coated copper grids (Nisshin EM Corporation, Tokyo, Japan) and negatively stained with 2% phosphotungstic acid solution (pH 5.8). All samples were examined with an H-7650 electron microscope at 80 kV (Hitachi, Kyoto, Japan) (Maruyama *et al.*, 2014).

Sucrose gradient sedimentation analysis

Sucrose gradient sedimentation analysis was performed as described previously (Suzuki *et al.*, 2012). Briefly, 3 dpt cells were harvested in 10 mM Tris-HCl (pH 7.5), 2 mM $MgCl_2$, and 0.25% Brij 58 (Sigma, St. Louis, MO). The cellular lysates were subjected to three cycles of freezing and thawing, and cellular debris was removed via centrifugation at 500 × *g* for 10 min at 4°C, and the resulting supernatants overlaid onto a preformed 30-50% sucrose gradient in 20 mM Tris-HCl (pH 8.0). Samples were centrifuged at 192,000 × *g* for 1 hr at 4°C (SW55 Ti rotor; Beckman Coulter, Brea, CA), each 400 μl fraction was taken from the top for 12 fractions. Each fraction was subjected to SDS-PAGE and immunoblotting with an anti-SV40 VP1 antibody overnight at 4°C. After washing the membrane with TBST, the membrane was incubated with the HRP-conjugated anti-rabbit IgG for 1 hr at room temperature (Biosource International). The immune complexes were detected, and the chemiluminescence signals were visualized.

JCV VLPs were prepared as previously described (Kobayashi *et al.*, 2013). In brief, BL21 (DE3) pLysS competent cells (Stratagene, La Jolla, CA) were transformed with the pET15b plasmid (Novagen, Madison, WI) encoding the full-length JCV VP1 gene, and VLPs were purified.

Results

Transfection of the VmPyV1 genome

To test whether the VmPyV1 genome produce viral proteins in cultured cells, the whole circular genome was transfected into HEK293T cells. At 4 dpt, the cells were harvested and examined for the presence of viral messenger RNAs (mRNAs) and proteins.

To identify TAg and VP1 mRNA transcripts specific for VmPyV1 in transfected cells, TAg and VP1 primers were generated. TAg primers were designed to cover a predicted splicing site of the early mRNA (Fig. 2, dotted line) (Johne & Müller, 2003). VmPyV1 TAg spliced mRNA transcripts and VP1 specific mRNA transcripts were both verified by RT-PCR (Fig. 4A). By RT-PCR for TAg, two closely separated PCR products were observed (approximately 1,200 and 800 bp in size) [Fig. 4A, upper panel, reverse transcription (RT) (+) lane 2]. Both bands were purified from an agarose gel and then directly sequenced. The sequence of the 1,200 bp PCR product was consistent with that of the VmPyV1 genome, suggesting that this PCR product was an unspliced TAg mRNA transcript. The sequence of the 800 bp PCR product was in accordance with the sequence of the VmPyV1 genome devoid of 4,542–4,938 nucleotides (Fig. 2, dotted line), thus suggesting that this PCR product was a spliced mRNA of VmPyV1 TAg. Since the HEK293T cells express the SV40 TAg (Soneoka *et al.*, 1995), I checked the sequence alignment between SV40 TAg and the spliced mRNA and confirmed that the 800 bp product was not derived from SV40 TAg. A PCR product was detected by RT-PCR for VP1, and the size of the product was similar to that of the PCR product from the VmPyV1 genome (approximately 600 bp in size) [Fig. 4A, lower panel, RT (+) lanes 2 and 4]. The 800 bp spliced and 600 bp mRNA

(A)

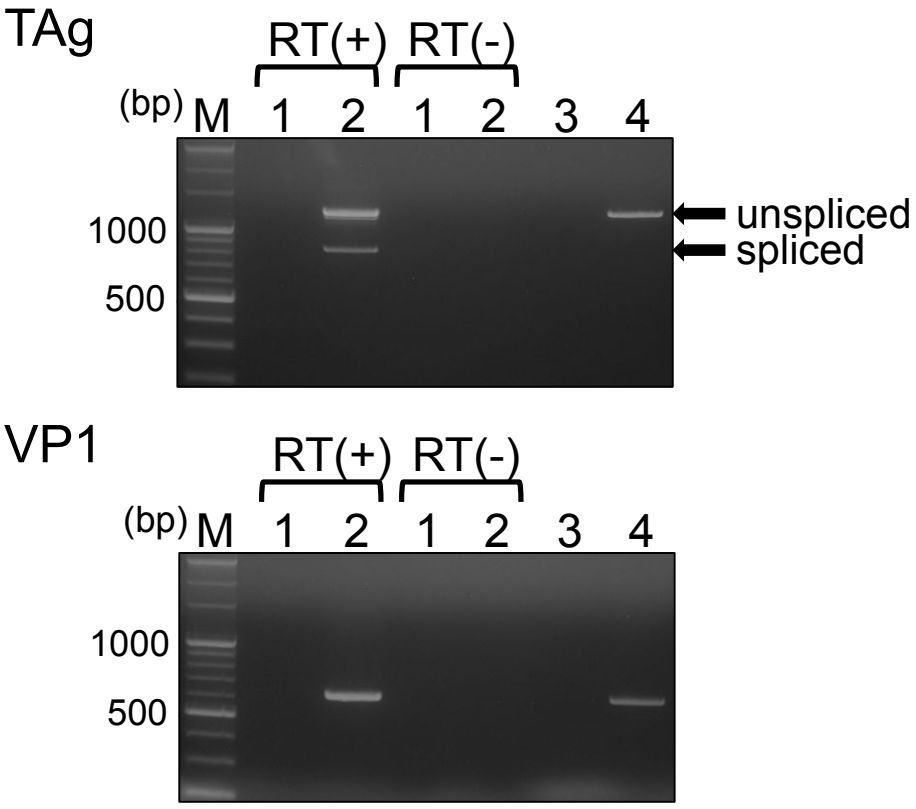
TAg
RT(+) RT(-)
(bp) M 1 2 1 2 3 4
1000
500
unspliced
spliced
VP1
RT(+) RT(-)
(bp) M 1 2 1 2 3 4
1000
500

(B)

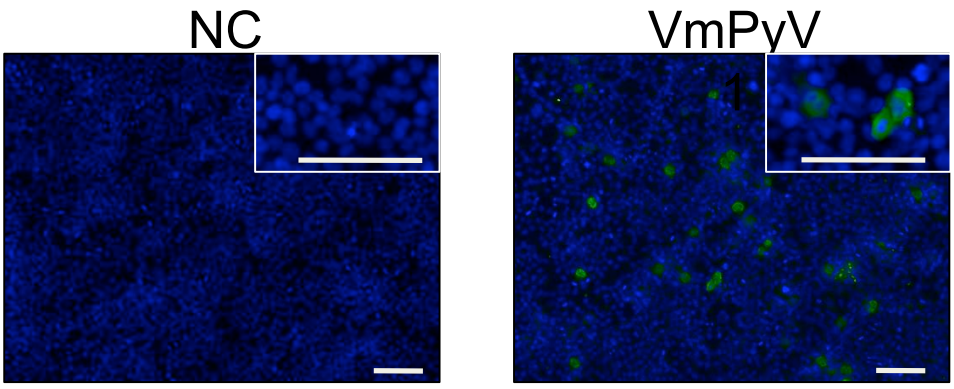
NC
VmPyV

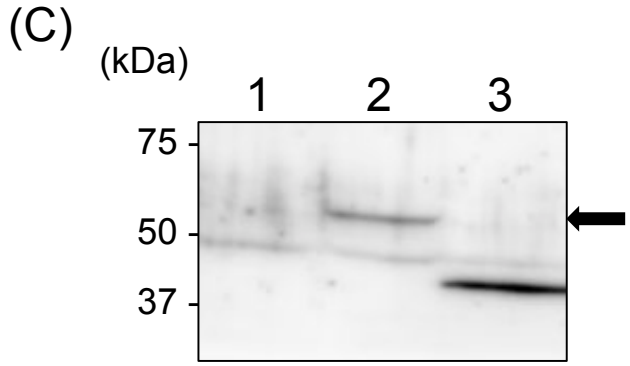

Figure 4. Expression of VmPyV1 mRNAs and protein in transfected HEK293T cells at 4 dpt. (A) RT-PCR analysis of TAg (upper panel) and VP1 (lower panel) mRNAs. Inclusion of reverse transcription [RT(+)] or not [RT(-); negative control] is indicated above the lanes. Lanes: M, 100 bp DNA ladder; 1, non-transfected HEK293T cells; 2, VmPyV1-transfected HEK293T cells; 3, sterile distilled water (negative control); 4, pUC19-VmPyV1 (positive control). (B) Immunocytochemical analysis of VmPyV1 VP1. NC, Non-transfected HEK293T cells (negative control); VmPyV1, VmPyV1-transfected HEK293T cells. VmPyV1 VP1 (green) was detected in the cell nuclei, which were counterstained with DAPI (blue). Insets show magnified views of the upper right section of each figure. Bars, 100 μm. (C) Immunoblot analysis of VmPyV1 VP1. Lanes: 1, non-transfected HEK293T cells (negative control); 2, VmPyV1-transfected HEK293T cells; 3, JCV-transfected HEK293T cells (positive control). The arrow indicates VmPyV1 VP1 (lane 2), with a molecular weight higher than that of JCV VP1 (lane 3).

transcripts were predicted to generate the viral TAg protein and VP1, respectively, in transfected cells.

To detect the protein expression and localization of VmPyV1 VP1 in transfected HEK293T cells, the immunocytochemical analysis was performed using an anti-SV40 VP1 antibody. I observed that the VmPyV1 VP1 was expressed and localized in the nuclei of some transfected cells at 4 dpt (Fig. 4B). To further confirm the antibody specificity and molecular weight of VmPyV1 VP1, I performed an immunoblot analysis. I was able to detect the VmPyV1 VP1 in transfected HEK293T cells and also found that its molecular weight was larger than that of JCV VP1 (positive control) (Fig. 4C, lanes 2 and 3). Overall, these results demonstrate that transfection of the VmPyV1 genome into HEK293T cells resulted in the expression of its viral proteins.

Expression of VmPyV1 VP1 in HEK293T cells

The full-length of VmPyV1 VP1 gene was amplified and cloned into the pCMV-FLAG vector [wild-type (WT) VmPyV1 VP1 (WT VP1)]. In addition, I synthesized the plasmid encoding a C-terminal deletion mutant of VmPyV1 VP1 (ΔC VP1). The deleted region was determined based on the amino acid sequence alignment with the reported PyV VP1s (Fig. 5). I made the ΔC VP1 (1-387 a.a. residues of WT VP1) with a stop codon (TAA), and cloned into the pCMV-FLAG vector. These plasmids were transfected into HEK293T cells individually and incubated for 48 hr. To detect the VP1 expression, I performed immunocytochemical analysis using an anti-SV40 VP1 antibody. Intracellular distribution of WT and ΔC VP1s were similar. Both WT and ΔC VP1s were mainly detected in the nuclei, also but a few, I confirmed VP1s in the cytoplasm of cells transfected with plasmid encoding WT or ΔC VP1 (Fig. 6A). I also performed immunoblot analysis to confirm the expression levels of WT and

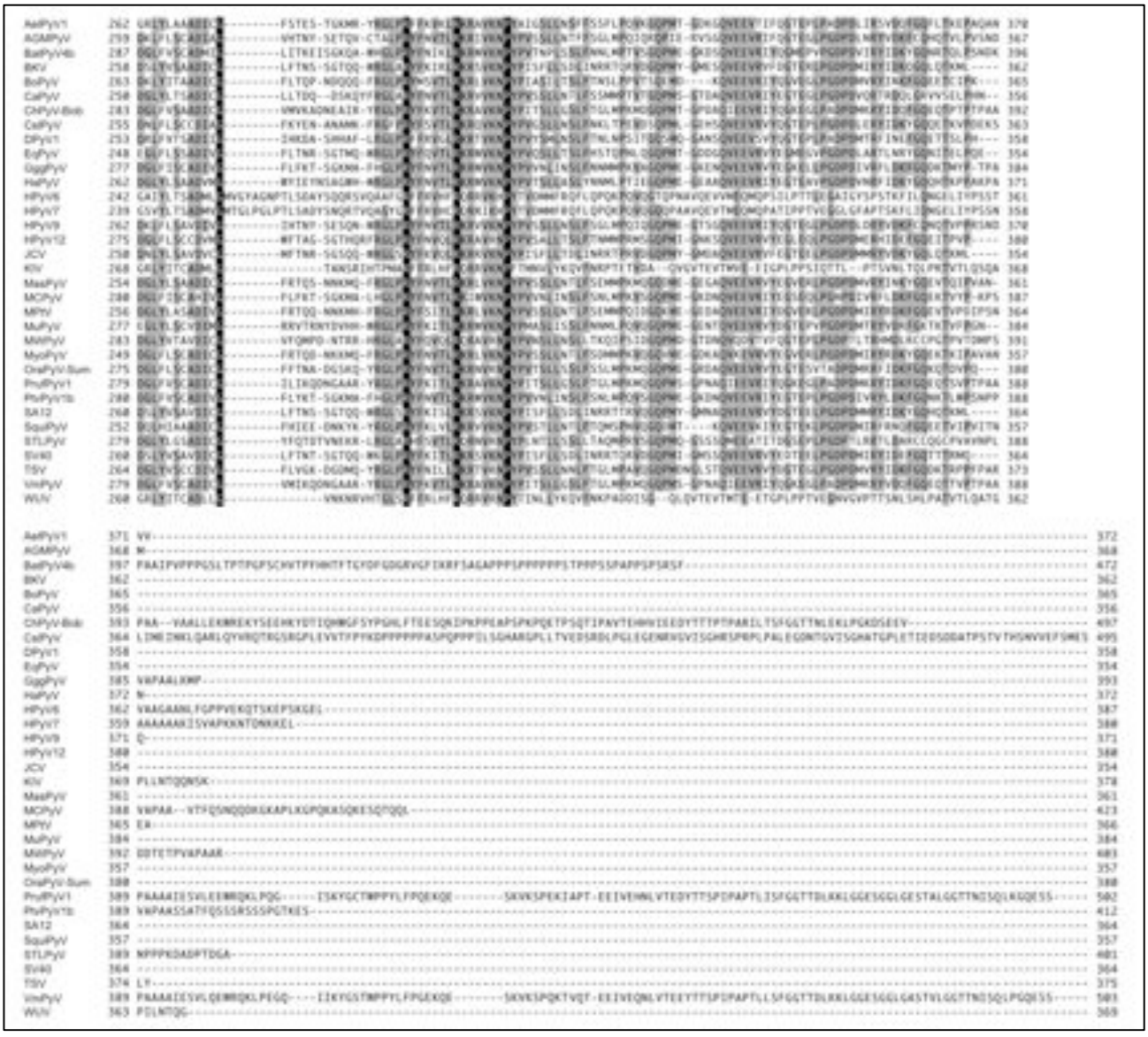

Figure 5. Alignment of PyV VP1s in C-terminal portions. Alignment of PyV VP1s in C-terminal portions with that of VmPyV1. The VP1 sequences of PyVs were obtained from GenBank (abbreviations and accession numbers are indicated in Table 1). Amino acid identities are shaded as follows: black shading indicates that all amino acid sequences were conserved, whereas grey shading indicates that more than 51% of them were conserved.

ΔC VP1s. I detected both WT and ΔC VP1s in the cells using the anti-SV40 VP1 antibody at the expected molecular weights of 56 and 44 kDa, respectively (Fig. 6B). Because ΔC VP1 lacks 388-503 amino acid residues of WT VP1 (116 a.a. deletion), its molecular weight is smaller than that of WT VP1. The expression levels of WT and ΔC VP1s were almost similar relative to the expression levels of internal control protein actin (Fig. 6B). These results suggested that the intracellular localization and expression levels of WT and ΔC VP1s were similar in the transfected cells.

Electron microscopical examination of VmPyV1 in HEK293T cells

Because the VmPyV1 VP1 was detected in transfected HEK293T cells, I investigated the formation of VLPs using transmission electron microscopy (TEM). At 2 dpt with WT and ΔC VP1-encoding plasmids, scraped cells were embedded in Epon resin and polymerized. Ultra-thin-sections with a thickness of 70 nm were stained with uranyl acetate and lead citrate. TEM revealed a large number of VLPs with a diameter of approximately 50 nm in the nuclei of WT VP1-expressing cells (WT VLPs; Fig. 7A-C). I also confirmed VLPs with a diameter of approximately 45-50 nm in the nuclei of ΔC VP1-expressing cells (ΔC VLPs; Fig. 7D-F); however, the number of ΔC VLPs was much lower than that of WT VLPs.

Sucrose gradient sedimentation analysis

To confirm that VLPs were formed by VmPyV1 VP1 in transfected cells, I also performed the sucrose gradient sedimentation analysis, which can distinguish VLPs from VP1 pentamers (Kawano *et al.*, 2006). As a positive control in the analysis, I used purified JCV VLPs (Kobayashi *et al.*, 2013). After ultracentrifugation, 12 fractions of 400 μl each were dispensed. Each fraction was analyzed by

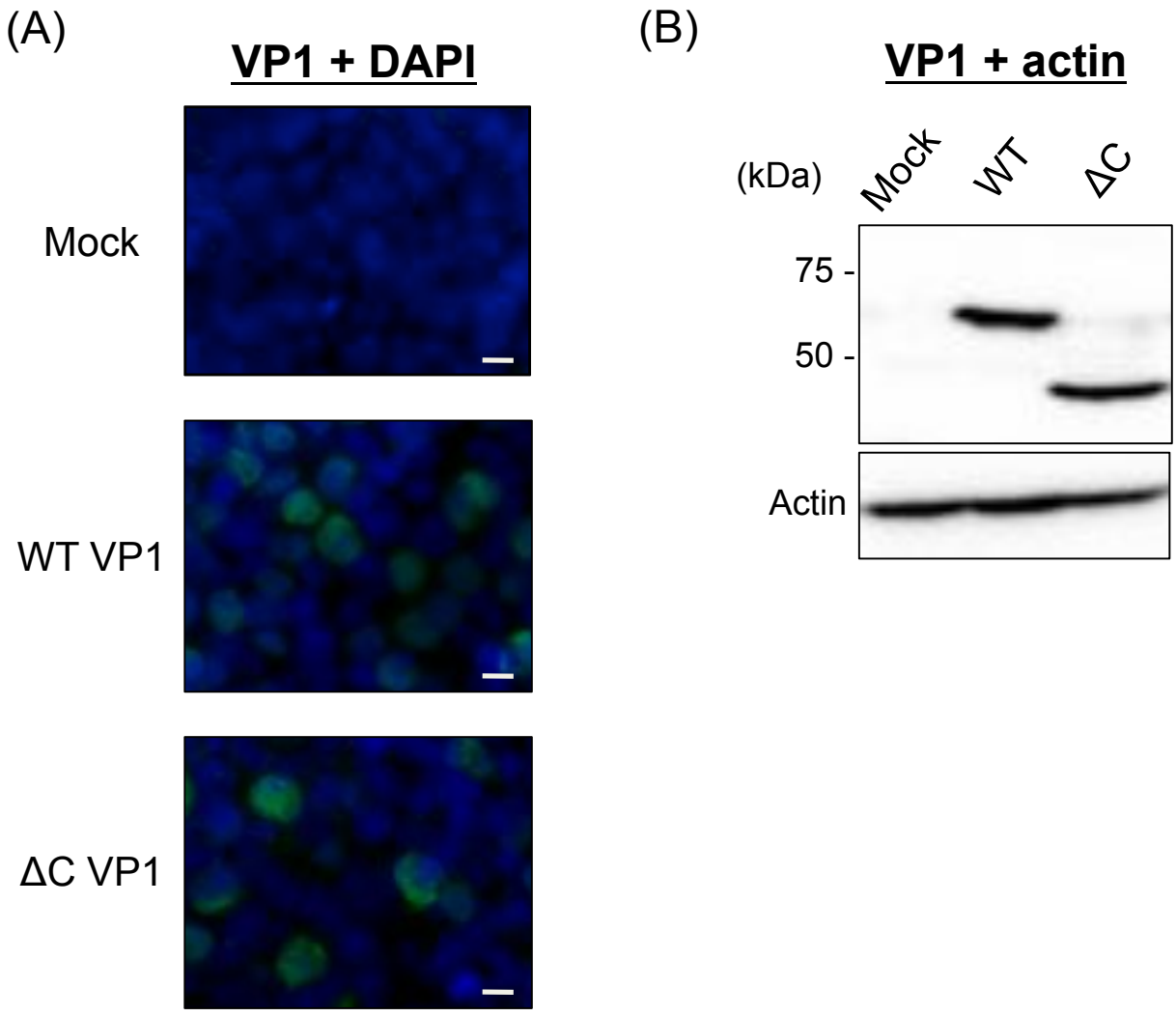

Figure 6. Expression of VmPyV1 VP1 protein in HEK293T cells. Immunocytochemical and immunoblot analyses of VmPyV1 VP1 with the anti-SV40 VP1 antibody. The HEK293T cells were transfected with WT VP1, ΔC VP1, or the corresponding empty vector (Mock) as a negative control. (A) VmPyV1 VP1 was detected colored in green. Cell nuclei were stained with DAPI (blue color). Scale bar, 10 nm. (B) WT and ΔC VP1 signals were detected in cellular lysates from HEK293T cells at the expected molecular weight positions in immunoblotting. Actin was used as a loading control.

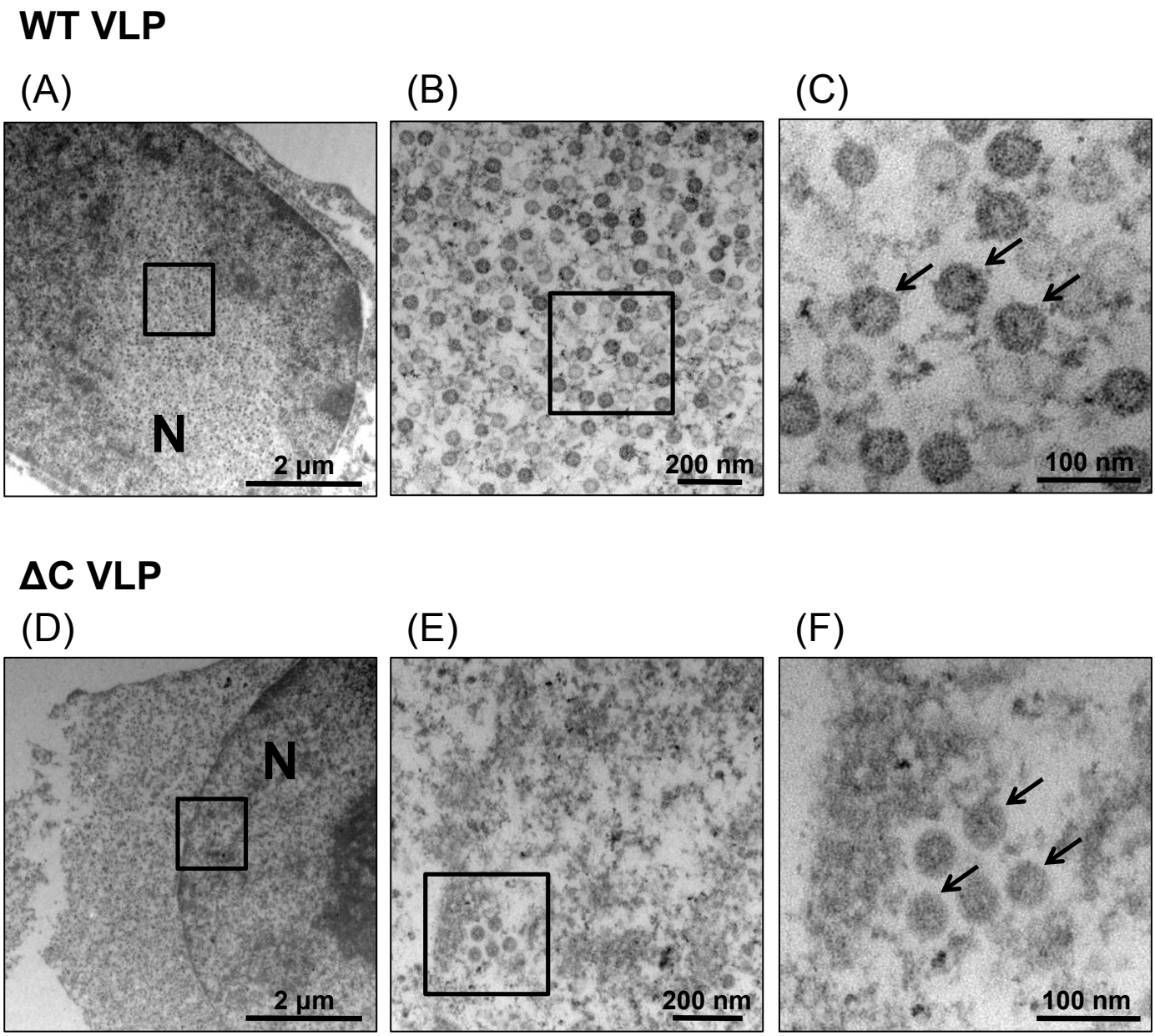

Figure 7. Electron micrographs of WT VP1 and ΔC VP1-expressing cells. Electron micrographs of HEK293T cells expressing WT VP1 (A-C) and ΔC VP1 (D-F). (B, C, E, and F) Higher magnification of the regions indicated in panels A, B, D, and E, respectively. All WT and ΔC VLPs were observed exclusively in the nuclei. The arrows indicate VLPs. N: nucleus.

immunoblotting with the anti-SV40 VP1 antibody. The VP1 signal in JCV VLPs was mainly detected in fractions 6 to 9 (Fig. 8A). The VP1 signal in cellular lysates from the WT VP1-expressing cells was also mainly detected in fractions 6 to 9 (Fig. 8B). However, the VP1 signal in cellular lysates from ΔC VP1-expressing cells was mainly detected in fractions 1 to 4, and slightly detected in fractions 5 to 8 (Fig. 8C). To confirm the formation of WT VLPs in fractions 6 to 9, I collected these fractions and verified them with negative-stained TEM. I observed a large number of WT VLPs with a diameter of approximately 50 nm (Fig. 8D). I also confirmed the presence of JCV VLPs in fractions 6 to 9 (data not shown).

(A) JCV VLPs

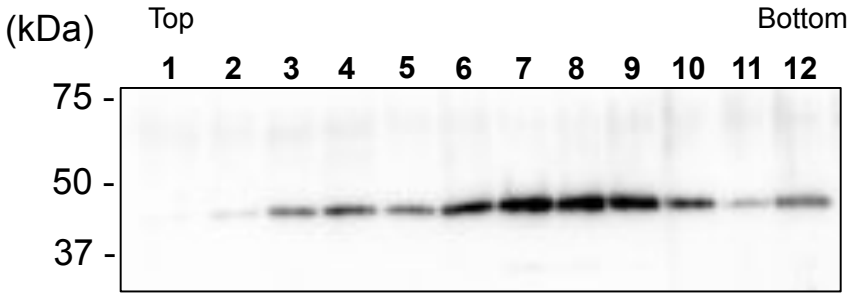

(B) WT VP1

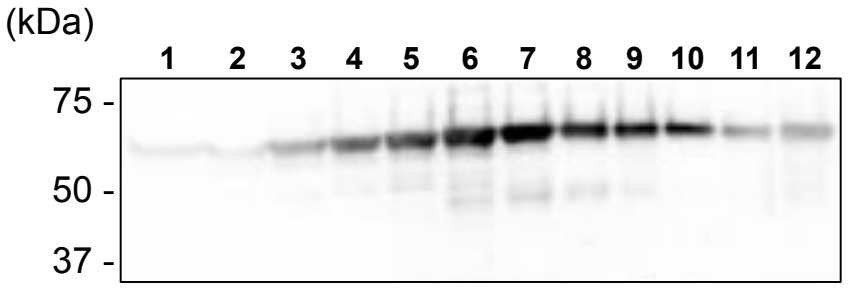

(C) ΔC VP1

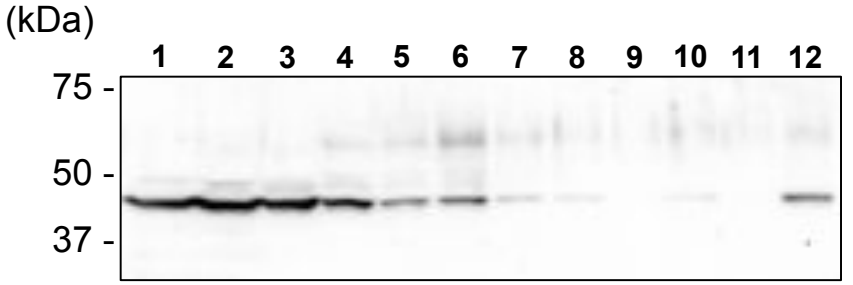

(D)

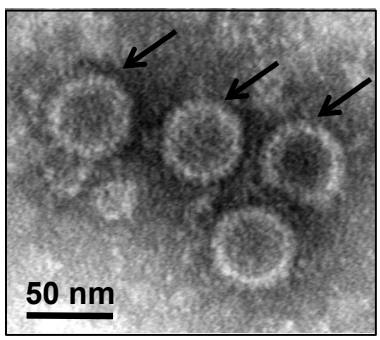

Figure 8. Sucrose gradient sedimentation analyses. (A-C) Immunoblot analyses of VP1 in fractionated samples after sucrose gradient sedimentation of JCV VLPs and cellular lysates from HEK293T cells expressing WT VP1 or ΔC VP1. Cellular lysates were separated by 30-50% sucrose gradient sedimentation and fractionated into 12 fractions from the tops of the tubes. The 12 fractions were further separated by SDS-PAGE and subjected to immunoblotting with the anti-SV40 VP1 antibody. (A) Purified JCV VLPs expressed in *E. coli*. (B) HEK293T cell lysates transfected with WT VP1 and (C) ΔC VP1. (D) Electron micrograph of negative staining of fractions 6 to 9 from HEK293T cells transfected with WT VP1. The arrows indicate VmPyV1 VLPs.

Discussion

VmPyV1 was originally detected in a VMS using nested broad-spectrum PCR techniques. It has a longer VP1 ORF in the C-terminus region compared with the sequences of other known PyVs VP1s, whereas its functions are still unclear. In general, the PyV capsid contains 360 molecules of VP1 formed with 72 pentamers, contain 5 molecules of VP1 and 1 molecule of VP2/VP3 (Liddington *et al.*, 1991; Stehle *et al.*, 1996).

In chapter 2, I detected transient mRNA expression of TAg and VP1 in HEK293T cells transfected with the whole circular VmPyV1 genome (Fig. 4A). The VP1 was also detectable by immunocytochemical and immunoblot analyses in transfected HEK293T cells at 4 dpt (Figs. 4B and C). I observed that VP1 was predominantly present in the enlarged cell nuclei, and the molecular weight of VmPyV1 VP1 was found to be approximately 55 kDa (Fig. 4C, lane 2), which is larger than that of JCV (40 kDa; Fig. 4C, lane 3); this difference in weight was probably due to the presence of the extra C-terminal tail. Similarly, in VmPyV1-transfected COS-7 and Vero cells, I detected the TAg and VP1 mRNAs as well as the VP1 by RT-PCR and immunocytochemistry (data not shown).

Moreover, to examine the role of C-terminal of VmPyV1 VP1 in virion formation, VmPyV1 VLPs consisting of WT VP1 or ΔC VP1 were generated in HEK293T cells. Immunocytochemical analysis revealed that WT and ΔC VP1s were expressed in the transfected HEK293T cells (Fig. 6A). Both WT and ΔC VP1s were also detected at the expected molecular weights by immunoblot analysis (Fig. 6B). Furthermore, the expression level of VP1s was comparable between the cells expressing WT VP1 and that expressing ΔC VP1. Although VLPs were observed in WT and ΔC

VP1-expressing cells by using electron microscopy (Fig. 7), the number of WT VLPs was higher than that of ΔC VLPs in each transfected cell. WT and ΔC VLPs were observed in the nuclei; however, no VLPs were confirmed in the cytoplasm. In addition, although the plasmids were transfected in same conditions, the number of cells with WT VLPs was higher than that of cells with ΔC VLPs (data not shown). These results suggest that the WT VP1 can produce VLPs more efficiently than ΔC VP1. On the other hand, the WT and ΔC VLPs were morphologically indistinguishable. I also performed a sucrose gradient sedimentation analysis (Kawano *et al.*, 2006). Immunoblot analysis revealed that the signal of JCV VLPs was mainly detected in fractions 6 to 9 (Fig. 8A). The VP1 signal in cellular lysates from WT VP1-expressing cells was also mainly detected in fractions 6 to 9 (Fig. 8B). I confirmed the presence of JCV VLPs and WT VLPs in fractions 6 to 9 with negative-stained TEM (Fig. 8D). However, the VP1 signal in cellular lysates from ΔC VP1-expressing cells was mainly detected in fractions 1 to 4 (Fig. 8C). Because the protein density in fractions 1 to 4 is lower than that in fractions 6 to 9, it is supposed that the VP1 signal in fractions 1 to 4 may have represented the pentamers rather than VLPs. In addition, the faint VP1 signal in fractions 5 to 8 of cellular lysates from ΔC VP1-expressing cells may have represented VLPs. This result is convincing in light of the TEM results showing fewer VLPs in ΔC VP1-expressing cells (Fig. 7D-F). Taken together, the results showed that ΔC VP1 formed VLPs; however, the efficiency of VLP formation was lower than that of WT VP1.

It has been reported that the C-terminal arm of PyVs VP1 can be subdivided into three segments: ‘C helix’, ‘C insert’, and ‘C loop’ (Liddington *et al.*, 1991; Stehle *et al.*, 1996). The C helix of SV40 (SFLLSDLINRRTQ; 305-317 a.a.) mediates contacts between pentamers as described previously (Liddington *et al.*, 1991; Stehle *et al.*,

1996). As demonstrated in Fig. 5, the C helix of SV40 is predicted to correspond to the 295-307 amino acid residues (SFLLTDLINRRTP) of JCV, and the 325-337 amino acid residues (TSLLGSLFTGLMP) of VmPyV1. In comparison among three viruses, the homology was 85% for SV40-JCV, 23% for SV40-VmPyV1, and 31% for JCV-VmPyV1 in the C helix of VP1s. It revealed that the C helix of JCV may mediate contacts between pentamers because of the high homology with that of SV40. However, the C helix of VmPyV1 has low homology with that of SV40 and JCV. As shown in Fig. 7, I observed that the number of WT VLPs was much higher than that of ΔC VLPs. Thus, the deleted C-terminal 116 amino acid residues (388-503 a.a.) of VmPyV1 VP1 affect the efficiency of its VLP formation rather than the expected C helix of VmPyV1.

ChPyV also encodes a unique extended C-terminal VP1 of 497 a.a., and ChPyV VLPs were expressed with a diameter of approximately 45 nm (Zielonka *et al.*, 2011). The diameter of VmPyV1 WT VLPs is approximately 50 nm (Fig. 8D). These results suggest that the length of VP1 amino acid residues has no effect on the size (i.e., diameter) of VLPs. It has been reported that SV40 VLPs made exclusively of VP1 and native SV40 virions were morphologically indistinguishable under electron microscopy (Kosukegawa *et al.*, 1996). I observed that VmPyV1 VLPs have a typical shape of PyV virions, and their diameters were approximately 50 nm in size, suggesting that native VmPyV1 virions also have morphology similar to that of its VLPs.

In conclusion, I detected VP1 expression in the transfected HEK293T cells by immunocytochemical and immunoblot analyses. Moreover, I demonstrated that VmPyV1 VLPs were formed in mammalian cells expressing VP1, and found the extra C-terminal region of VP1 does not affect the size and morphology of VLPs. The

C-terminal of VmPyV1 VP1 may have some function for efficient VLP formation. Further studies to investigate of function(s) of the extra C-terminal region of VmPyV1 VP1 need to be continued.

Summary

Recently, I detected novel vervet monkey polyomavirus 1 (VmPyV1) in a VM. Among amino acid sequences of major capsid protein VP1s of other PyVs, VmPyV1 VP1 is the longest, with additional amino acid residues in the C-terminal region. To examine whether the VmPyV1 genome could produce viral proteins in cultured cells, the whole genome was transfected into HEK293T cells. I detected VP1 in expression in the transfected HEK293T cells by immunocytochemical and immunoblot analyses.

Moreover, to examine the role of extended C-terminal of VmPyV1 VP1 in virion formation, I generated VLPs of VmPyV1 VP1 because VLP is a useful tool for the investigation of the morphological characters of PyV virions. After the full-length VmPyV1 VP1 was subcloned into a mammalian expression plasmid, the plasmid was transfected into HEK293T cells. Thereafter, WT VLPs were purified from the cell lysates of the transfected cells via sucrose gradient sedimentation. Electron microscopic analyses revealed that VmPyV1 VP1 forms VLPs with a diameter of approximately 50 nm that are exclusively localized in cell nuclei. Furthermore, I generated ΔC VLPs consisting of the deletion mutant VmPyV1 VP1 lacking the C-terminal 116 amino acid residues, and compared its VLP formation efficiency and morphology to WT VLPs. WT and ΔC VLPs were similar in size, but the number of ΔC VLPs was much lower than that of WT VLPs in VP1-expressing HEK293T cells. These results suggest that the length of VP1 is unrelated to virion morphology; however, the C-terminal region of VmPyV1 VP1 affects the efficiency of its VLP formation.

General Conclusion

Recently, emerging and reemerging infectious diseases, including zoonoses, are constantly appearing worldwide, and become a major concern to public health for humans and nonhumans. Because of increased contact between humans and wildlife, the appearance of zoonotic pathogens in human populations is increased.

PyV infection occurs during early childhood, and causes subclinical infections with lifelong persistence in their natural nonimmunocompromised hosts. When the host immunity-compromised AIDS patients and organ transplant recipients, the viruses can be reactivated and cause diseases, such as nephropathy and PML. It is controversial as to whether PyVs can be transmitted from wild animals to humans and thereafter cause disease. To examine potential threats of the zoonotic transfer of PyVs between NHPs and humans, the surveillance of PyVs in wildlife is important. In this thesis, I examined PyVs in wild NHPs in Zambia with permission from the ZAWA.

In chapter 1, I analyzed 200 DNA samples from the spleens and kidneys of NHPs (n = 100). I detected seven PyV genome fragments (7/200; 3.5%), and identified five full-length viral genomes. Phylogenetic analysis revealed that four PyVs were closely related to known PyVs, AGMPyV and SA12. Only one virus detected from a VMS was found to be related, with relatively low nucleotide sequence identity (74%), to the ChPyV, which shares 48% nucleotide sequence identity with the human MCPyV identified from MCC. This virus was named vervet monkey PyV 1 (VmPyV1) as a novel PyV.

In chapter 2, I focused on further characterization of the VmPyV1. To examine whether the VmPyV1 genome produce viral proteins in cultured cells, the whole VmPyV1 genome was transfected into HEK293T cells. I detected VP1 in expression in

the transfected HEK293T cells. Because VmPyV1 encodes the unique extended C-terminal VP1, I generated VLPs to examine the role of VmPyV1 VP1 in virion formation. Furthermore, I generated VLPs consisting of the ΔC VP1 lacking the C-terminal 116 amino acid residues, and compared its VLP formation efficiency and morphology to those of VLPs from WT VP1. WT and ΔC VLPs were similar in size, but the number of ΔC VLPs was much lower than that of WT VLPs in VP1-expressing HEK293T cells. These results suggest that the length of VP1 is unrelated to virion morphology; however, the C-terminal region of VmPyV1 VP1 affects the efficiency of its VLP formation.

In this thesis, I detected PyV genomes in NHPs in Zambia and also identified a novel PyV, which was designated as VmPyV1. Moreover, I confirmed the formation of VLPs in the transfected HEK293T cells with the plasmid encoding the VmPyV1 VP1. Although the pathogenicity of VmPyV1 and function(s) of the extra C-terminal region of VmPyV1 are still unclear, these findings provided information about the PyV prevalence in NHPs in Zambia and the C-terminal of VmPyV1 VP1 may have some function for efficient VLP formation. The surveillance of wildlife needs to be continued to examine the transmission possibility of infection agents.

References

Allander, T., Andreasson, K., Gupta, S., Bjerkner, A., Bogdanovic, G., Persson, M. A., Dalianis, T., Ramqvist, T. & Andersson, B. (2007). Identification of a third human polyomavirus. *J Virol* **81**, 4130-4136.

Anthony, S. J., St Leger, J. A., Navarrete-Macias, I., Nilson, E., Sanchez-Leon, M., Liang, E., Seimon, T., Jain, K., Karesh, W., Daszak, P., Briese, T. & Lipkin, W. I. (2013). Identification of a novel cetacean polyomavirus from a common dolphin (Delphinus delphis) with Tracheobronchitis. *PLoS One* **8**, e68239.

Bergsagel, D. J., Finegold, M. J., Butel, J. S., Kupsky, W. J. & Garcea, R. L. (1992). DNA sequences similar to those of simian virus 40 in ependymomas and choroid plexus tumors of childhood. *N Engl J Med* **326**, 988-993.

Bofill-Mas, S., Rodriguez-Manzano, J., Calgua, B., Carratala, A. & Girones, R. (2010). Newly described human polyomaviruses Merkel cell, KI and WU are present in urban sewage and may represent potential environmental contaminants. *Virol J* **7**, 141.

Braun, L., Kalter, S. S., Yakovleva, L. A., Kaschula, V. R. & Shah, K. V. (1980). Neutralizing antibodies to simian papovavirus SA12 in Old World primates in laboratory colonies: high prevalence in baboons. *J Med Primatol* **9**, 240-246.

Buck, C. B., Phan, G. Q., Raiji, M. T., Murphy, P. M., McDermott, D. H. & McBride, A. A. (2012). Complete Genome Sequence of a Tenth Human Polyomavirus. *Journal of Virology* **86**, 10887-10887.

Cantalupo, P., Doering, A., Sullivan, C. S., Pal, A., Peden, K. W., Lewis, A. M. & Pipas, J. M. (2005). Complete nucleotide sequence of polyomavirus SA12. *J Virol* **79**, 13094-13104.

Chang, D., Fung, C. Y., Ou, W. C., Chao, P. C., Li, S. Y., Wang, M., Huang, Y. L., Tzeng, T. Y. & Tsai, R. T. (1997). Self-assembly of the JC virus major capsid protein, VP1, expressed in insect cells. *J Gen Virol* **78 (Pt 6)**, 1435-1439.

Chen, P. L., Wang, M., Ou, W. C., Lii, C. K., Chen, L. S. & Chang, D. (2001). Disulfide bonds stabilize JC virus capsid-like structure by protecting calcium ions from chelation. *FEBS Lett* **500**, 109-113.

Deuzing, I., Fagrouch, Z., Groenewoud, M. J., Niphuis, H., Kondova, I., Bogers, W. & Verschoor, E. J. (2010). Detection and characterization of two chimpanzee polyomavirus genotypes from different subspecies. *Virol J* **7**, 347.

Fagrouch, Z., Sarwari, R., Lavergne, A., Delaval, M., de Thoisy, B., Lacoste, V. & Verschoor, E. J. (2012). Novel polyomaviruses in South American bats and their relationship to other members of the family Polyomaviridae. *J Gen Virol* **93**, 2652-2657.

Felsenstein, J. (1985). Confidence limits on phylogenies: an approach using the bootstrap. *Evolution* **39**, 783-791.

Feng, H., Shuda, M., Chang, Y. & Moore, P. S. (2008). Clonal integration of a polyomavirus in human Merkel cell carcinoma. *Science* **319**, 1096-1100.

Gaynor, A. M., Nissen, M. D., Whiley, D. M., Mackay, I. M., Lambert, S. B., Wu, G., Brennan, D. C., Storch, G. A., Sloots, T. P. & Wang, D. (2007). Identification of a novel polyomavirus from patients with acute respiratory tract infections. *PLoS Pathog* **3**, e64.

Hockings, K. J., Yamakoshi, G., Kabasawa, A. & Matsuzawa, T. (2010). Attacks on local persons by chimpanzees in Bossou, Republic of Guinea: long-term perspectives. *Am J Primatol* **72**, 887-896.

Imperiale, M. J. & Major, E. O. (2007). Polyomaviruses. *Fields virology* **2**,

2268-2282.

Jiang, M., Abend, J. R., Johnson, S. F. & Imperiale, M. J. (2009). The role of polyomaviruses in human disease. *Virology* **384**, 266-273.

Johne, R., Enderlein, D., Nieper, H. & Müller, H. (2005). Novel polyomavirus detected in the feces of a chimpanzee by nested broad-spectrum PCR. *J Virol* **79**, 3883-3887.

Johne, R. & Müller, H. (2003). The genome of goose hemorrhagic polyomavirus, a new member of the proposed subgenus Avipolyomavirus. *Virology* **308**, 291-302.

Johne, R. & Müller, H. (2007). Polyomaviruses of birds: etiologic agents of inflammatory diseases in a tumor virus family. *J Virol* **81**, 11554-11559.

Kasamatsu, H. & Nehorayan, A. (1979). Intracellular localization of viral polypeptides during simian virus 40 infection. *J Virol* **32**, 648-660.

Kawano, M. A., Inoue, T., Tsukamoto, H., Takaya, T., Enomoto, T., Takahashi, R. U., Yokoyama, N., Yamamoto, N., Nakanishi, A., Imai, T., Wada, T., Kataoka, K. & Handa, H. (2006). The VP2/VP3 minor capsid protein of simian virus 40 promotes the in vitro assembly of the major capsid protein VP1 into particles. *J Biol Chem* **281**, 10164-10173.

Kean, J. M., Rao, S., Wang, M. & Garcea, R. L. (2009). Seroepidemiology of human polyomaviruses. *PLoS Pathog* **5**, e1000363.

Klein, G., Powers, A. & Croce, C. (2002). Association of SV40 with human tumors. *Oncogene* **21**, 1141-1149.

Knowles, W. A. (2006). Discovery and epidemiology of the human polyomaviruses BK virus (BKV) and JC virus (JCV). *Adv Exp Med Biol* **577**, 19-45.

Kobayashi, S., Orba, Y., Yamaguchi, H., Kimura, T. & Sawa, H. (2012).

Accumulation of ubiquitinated proteins is related to West Nile virus-induced neuronal apoptosis. *Neuropathology* **32**, 398-405.

Kobayashi, S., Suzuki, T., Igarashi, M., Orba, Y., Ohtake, N., Nagakawa, K., Niikura, K., Kimura, T., Kasamatsu, H. & Sawa, H. (2013). Cysteine Residues in the Major Capsid Protein, Vp1, of the JC Virus Are Important for Protein Stability and Oligomer Formation. *PLoS One* **8**, e76668.

Korup, S., Rietscher, J., Calvignac-Spencer, S., Trusch, F., Hofmann, J., Moens, U., Sauer, I., Voigt, S., Schmuck, R. & Ehlers, B. (2013). Identification of a novel human polyomavirus in organs of the gastrointestinal tract. *PLoS One* **8**, e58021.

Kosukegawa, A., Arisaka, F., Takayama, M., Yajima, H., Kaidow, A. & Handa, H. (1996). Purification and characterization of virus-like particles and pentamers produced by the expression of SV40 capsid proteins in insect cells. *Biochim Biophys Acta* **1290**, 37-45.

Krumbholz, A., Bininda-Emonds, O. R., Wutzler, P. & Zell, R. (2009). Phylogenetics, evolution, and medical importance of polyomaviruses. *Infect Genet Evol* **9**, 784-799.

Lednicky, J. A., Garcea, R. L., Bergsagel, D. J. & Butel, J. S. (1995). Natural simian virus 40 strains are present in human choroid plexus and ependymoma tumors. *Virology* **212**, 710-717.

Leendertz, F. H., Scuda, N., Cameron, K. N., Kidega, T., Zuberbühler, K., Leendertz, S. A., Couacy-Hymann, E., Boesch, C., Calvignac, S. & Ehlers, B. (2011). African great apes are naturally infected with polyomaviruses closely related to Merkel cell polyomavirus. *J Virol* **85**, 916-924.

Liddington, R. C., Yan, Y., Moulai, J., Sahli, R., Benjamin, T. L. & Harrison, S. C.

(1991). Structure of simian virus 40 at 3.8-A resolution. *Nature* **354**, 278-284.

Lim, E. S., Reyes, A., Antonio, M., Saha, D., Ikumapayi, U. N., Adeyemi, M., Stine, O. C., Skelton, R., Brennan, D. C., Mkakosya, R. S., Manary, M. J., Gordon, J. I. & Wang, D. (2013). Discovery of STL polyomavirus, a polyomavirus of ancestral recombinant origin that encodes a unique T antigen by alternative splicing. *Virology* **436**, 295-303.

Maruyama, J., Miyamoto, H., Kajihara, M., Ogawa, H., Maeda, K., Sakoda, Y., Yoshida, R. & Takada, A. (2014). Characterization of the envelope glycoprotein of a novel filovirus, lloviu virus. *J Virol* **88**, 99-109.

Noda, T., Sagara, H., Suzuki, E., Takada, A., Kida, H. & Kawaoka, Y. (2002). Ebola virus VP40 drives the formation of virus-like filamentous particles along with GP. *J Virol* **76**, 4855-4865.

Orba, Y., Kobayashi, S., Nakamura, I., Ishii, A., Hang'ombe, B. M., Mweene, A. S., Thomas, Y., Kimura, T. & Sawa, H. (2011). Detection and characterization of a novel polyomavirus in wild rodents. *J Gen Virol* **92**, 789-795.

Ou, W. C., Wang, M., Fung, C. Y., Tsai, R. T., Chao, P. C., Hseu, T. H. & Chang, D. (1999). The major capsid protein, VP1, of human JC virus expressed in Escherichia coli is able to self-assemble into a capsid-like particle and deliver exogenous DNA into human kidney cells. *J Gen Virol* **80 (Pt 1)**, 39-46.

Pawlita, M., Clad, A. & zur Hausen, H. (1985). Complete DNA sequence of lymphotropic papovavirus: prototype of a new species of the polyomavirus genus. *Virology* **143**, 196-211.

Pipas, J. M. (2009). SV40: Cell transformation and tumorigenesis. *Virology* **384**, 294-303.

Ramqvist, T. & Dalianis, T. (2009). Murine polyomavirus tumour specific transplantation antigens and viral persistence in relation to the immune response, and tumour development. *Semin Cancer Biol* **19**, 236-243.

Saitou, N. & Nei, M. (1987). The neighbor-joining method: a new method for reconstructing phylogenetic trees. *Mol Biol Evol* **4**, 406-425.

Sasaki, M., Ishii, A., Orba, Y., Thomas, Y., Hang'ombe, B. M., Moonga, L., Mweene, A. S., Ogawa, H., Nakamura, I., Kimura, T. & Sawa, H. (2013). Human parainfluenza virus type 3 in wild nonhuman primates, Zambia. *Emerg Infect Dis* **19,** 1500-1503.

Schowalter, R. M., Pastrana, D. V., Pumphrey, K. A., Moyer, A. L. & Buck, C. B. (2010). Merkel cell polyomavirus and two previously unknown polyomaviruses are chronically shed from human skin. *Cell Host Microbe* **7**, 509-515.

Scuda, N., Hofmann, J., Calvignac-Spencer, S., Ruprecht, K., Liman, P., Kühn, J., Hengel, H. & Ehlers, B. (2011). A novel human polyomavirus closely related to the african green monkey-derived lymphotropic polyomavirus. *J Virol* **85**, 4586-4590.

Scuda, N., Madinda, N. F., Akoua-Koffi, C., Adjogoua, E. V., Wevers, D., Hofmann, J., Cameron, K. N., Leendertz, S. A., Couacy-Hymann, E., Robbins, M., Boesch, C., Jarvis, M. A., Moens, U., Mugisha, L., Calvignac-Spencer, S., Leendertz, F. H. & Ehlers, B. (2013). Novel polyomaviruses of nonhuman primates: genetic and serological predictors for the existence of multiple unknown polyomaviruses within the human population. *PLoS Pathog* **9**, e1003429.

Shen, P. S., Enderlein, D., Nelson, C. D., Carter, W. S., Kawano, M., Xing, L., Swenson, R. D., Olson, N. H., Baker, T. S., Cheng, R. H., Atwood, W. J.,

Johne, R. & Belnap, D. M. (2011). The structure of avian polyomavirus reveals variably sized capsids, non-conserved inter-capsomere interactions, and a possible location of the minor capsid protein VP4. *Virology* **411**, 142-152.

Siebrasse, E. A., Reyes, A., Lim, E. S., Zhao, G., Mkakosya, R. S., Manary, M. J., Gordon, J. I. & Wang, D. (2012). Identification of MW polyomavirus, a novel polyomavirus in human stool. *J Virol* **86**, 10321-10326.

Soneoka, Y., Cannon, P. M., Ramsdale, E. E., Griffiths, J. C., Romano, G., Kingsman, S. M. & Kingsman, A. J. (1995). A transient three-plasmid expression system for the production of high titer retroviral vectors. *Nucleic Acids Res* **23**, 628-633.

Sroller, V., Hamšíková, E., Ludvíková, V., Vochozková, P., Kojzarová, M., Fraiberk, M., Saláková, M., Morávková, A., Forstová, J. & Němečková, S. (2013). Seroprevalence rates of BKV, JCV, and MCPyV polyomaviruses in the general Czech Republic population. *J Med Virol*, in press.

Stehle, T., Gamblin, S. J., Yan, Y. & Harrison, S. C. (1996). The structure of simian virus 40 refined at 3.1 A resolution. *Structure* **4**, 165-182.

Stevens, H., Bertelsen, M. F., Sijmons, S., Van Ranst, M. & Maes, P. (2013). Characterization of a Novel Polyomavirus Isolated from a Fibroma on the Trunk of an African Elephant (Loxodonta africana). *PLOS ONE* **8**, e77884.

Suzuki, T., Orba, Y., Makino, Y., Okada, Y., Sunden, Y., Hasegawa, H., Hall, W. W. & Sawa, H. (2013). Viroporin activity of the JC polyomavirus is regulated by interactions with the adaptor protein complex 3. *Proc Natl Acad Sci U S A* **110**, 18668-18673.

Suzuki, T., Orba, Y., Okada, Y., Sunden, Y., Kimura, T., Tanaka, S., Nagashima, K., Hall, W. W. & Sawa, H. (2010). The human polyoma JC virus

agnoprotein acts as a viroporin. *PLoS Pathog* **6**, e1000801.

Suzuki, T., Semba, S., Sunden, Y., Orba, Y., Kobayashi, S., Nagashima, K., Kimura, T., Hasegawa, H. & Sawa, H. (2012). Role of JC virus agnoprotein in virion formation. *Microbiol Immunol* **56**, 639-646.

Tamura, K., Peterson, D., Peterson, N., Stecher, G., Nei, M. & Kumar, S. (2011). MEGA5: molecular evolutionary genetics analysis using maximum likelihood, evolutionary distance, and maximum parsimony methods. *Mol Biol Evol* **28**, 2731-2739.

Tolstov, Y. L., Pastrana, D. V., Feng, H., Becker, J. C., Jenkins, F. J., Moschos, S., Chang, Y., Buck, C. B. & Moore, P. S. (2009). Human Merkel cell polyomavirus infection II. MCV is a common human infection that can be detected by conformational capsid epitope immunoassays. *Int J Cancer* **125**, 1250-1256.

van der Meijden, E., Janssens, R. W., Lauber, C., Bouwes Bavinck, J. N., Gorbalenya, A. E. & Feltkamp, M. C. (2010). Discovery of a new human polyomavirus associated with trichodysplasia spinulosa in an immunocompromized patient. *PLoS Pathog* **6**, e1001024.

Wellehan, J. F., Rivera, R., Archer, L. L., Benham, C., Muller, J. K., Colegrove, K. M., Gulland, F. M., St Leger, J. A., Venn-Watson, S. K. & Nollens, H. H. (2011). Characterization of California sea lion polyomavirus 1: expansion of the known host range of the Polyomaviridae to Carnivora. *Infect Genet Evol* **11**, 987-996.

Yamaguchi, H., Kobayashi, S., Ishii, A., Ogawa, H., Nakamura, I., Moonga, L., Hang'ombe, B. M., Mweene, A. S., Thomas, Y., Kimura, T., Sawa, H. & Orba, Y. (2013). Identification of a novel polyomavirus from vervet monkeys

in Zambia. *J Gen Virol* **94**, 1357-1364.

Yu, G., Greninger, A. L., Isa, P., Phan, T. G., Martínez, M. A., de la Luz Sanchez, M., Contreras, J. F., Santos-Preciado, J. I., Parsonnet, J. & Miller, S. (2012). Discovery of a Novel Polyomavirus in Acute Diarrheal Samples from Children. *PloS one* **7**, e49449.

Zielonka, A., Verschoor, E. J., Gedvilaite, A., Roesler, U., Müller, H. & Johne, R. (2011). Detection of chimpanzee polyomavirus-specific antibodies in captive and wild-caught chimpanzees using yeast-expressed virus-like particles. *Virus Res* **155**, 514-519.

Acknowledgements

I would like to acknowledge Professor Hirofumi Sawa, Division of Molecular Pathobiology, Research Center for Zoonosis Control, Hokkaido University, for his valuable advices and detailed review of this manuscript.

Great appreciation is extended to Professor Ayato Takada, Division of Global Epidemiology, Research Center for Zoonosis Control, Hokkaido University, Professor Hideaki Higashi, Division of Infection and Immunity, Research Center for Zoonosis Control, Hokkaido University, and Professor Takashi Kimura, Laboratory of Comparative Pathology, Department of Veterinary Clinical Sciences, Graduate School of Veterinary Medicine, Hokkaido University, for reviewing the manuscript, valuable advices, and suggestions.

I am also deeply grateful to Assistant Professor Yasuko Orba and Dr. Shintaro Kobayashi, Division of Molecular Pathobiology, Research Center for Zoonosis Control, Hokkaido University, for valuable advices, suggestions, and encouragement throughout this study.

I would like to acknowledge Professor Harumi Kasamatsu, Department of Molecular, Cell and Developmental Biology and Molecular Biology Institute, University of California at Los Angeles, for providing the polyclonal anti-SV40 VP1 antibody.

Very special thanks to my friends, Ms. Midori Inoue, Ms. Aiko Ohnuma, Dr.

Masahiro Kajihara, Mr. Osamu Noyori, Mr. Makoto Kuroda, Mr. Masayuki Hirata, Mr. Satoshi Fujiyoshi, and “Madogiwa” members, for encouraging and inspiring me and spending wonderful time.

Finally, thanks are also due to all members of the Division of Molecular Pathobiology, Research Center for Zoonosis Control, Hokkaido University.

Summary in Japanese

近年、新興・再興感染症が世界各地で発生し、公衆衛生上の問題となっている。地球環境の変化や貿易のグローバル化などにより、ヒトと野生動物との接触が増加し、自然界に由来する微生物がヒトに伝播する機会が増えた結果、人獣共通感染症が多発している。

ポリオーマウイルス（PyV）は小児期に無症候性に感染し、リンパ節などで初期増殖後、血行性に播種して諸臓器で持続感染する。その後、AIDS や臓器移植後などの免疫抑制状態において、PyV は再活性化して増殖し、BK ウイルス腎症や進行性多巣性白質脳症などに代表される病気を惹起する。野生動物が保有する PyV がヒトに伝播し、ヒトにおいて感染症を惹起するか否かに関しては結論が出ておらず、PyV の生活環については未だ不明な点が多い。このことから、自然界における既知及び未知の PyV を調査することは重要と考えられる。本研究は、アフリカのザンビア共和国における霊長類動物の PyV 感染状況を調査することを目的とした。

第一章では、PCR 法を用いてザンビア共和国の霊長類動物における PyV の感染状況を調査した。ザンビア野生動物保護局の許可の下、2009 年に Mfuwe 地域の Yellow baboon（YB）および Vervet monkey（VM）それぞれ 50 頭の脾臓・腎臓計 200 検体を採集し、各検体から DNA を抽出した。PyV の後期タンパク質である VP1 に対する broad-spectrum PCR 法を行い、PyV 遺伝子断片を検出し、断片の塩基配列を解読した。その結果、200 検体中 7 検体（3.5%）において、既存の PyV と相同性を有する遺伝子断片を確認した。これら PCR 陽性 7 検体において、Inverse PCR 法を用いてウイルスゲノム全長の単離を試み、5 種類の PyV ゲノム全長を単離した。系統学的解析の結果、4 種類は既知の PyV である African green monkey PyV と Simian agent 12 に近縁であることが判明した。しか

しながら、VM の脾臓検体から検出した 1 種類の PyV は、Chimpanzee PyV と低い相同性（74%）を有することを確認したため、新規 PyV、Vervet monkey PyV 1（VmPyV1）として報告した。また、既知の PyV とのアライメントの結果から、VmPyV1 は VP1 が既知の PyV と異なり、C 末端側に約 150 アミノ酸残基付加されていることが明らかになった。

第二章では、新規 PyV として同定した VmPyV1 に着目し、詳細な解析を実施した。VmPyV1 ゲノム全長を培養細胞に導入し、ウイルスタンパク質の産生を確認した。RT-PCR 法により前期タンパク質である TAg、及び VP1 の mRNA を確認し、免疫蛍光抗体法、ウエスタンブロット法にて VP1 が発現することを確認した。次に、VmPyV1 の粒子形成における VP1 の影響を、培養細胞を用いたウイルス様粒子（VLP）産生系を用いて、電子顕微鏡下で確認した。また、野生型（WT）の VLP だけでなく、C 末端領域を欠失させた変異体（ΔC）の VLP も同様に作製し、両者間における VLP の形態学的相違等を比較した。その結果、WT、ΔC 両者において直径約 50 nm の VLP の形成を培養細胞の核内に認めた。両者間における VLP の大きさ、形態に違いは認めなかったが、WT の VLP 数は ΔC と比較して顕著に多く、C 末端領域は粒子形成効率に関与することが示唆された。

本研究では、ザンビア共和国における霊長類動物の PyV 感染状況を調査した。その結果、計 200 検体のうち 7 検体（脾臓 5 検体、腎臓 2 検体）（3.5%）から PyV ゲノムを検出した。また、VM から新規 PyV として VmPyV1 を同定した。さらに、新規 VmPyV1 の VLP を作製し、VP1 の C 末端領域が、粒子形成効率に関与していることを明らかにした。今後も、PyV のヒト−動物間伝播についての情報を収集する為、サーベイランスを継続することが必要である。